Biome Renewables®

Biome Tidal Turbine Study

Final Report

May 31st, 2019

Team

Dr. Sue Molloy, Glas Ocean Engineering

Dr. Alison Mark, Consultant

Dr. Aaron MacNeill, Glas Ocean Engineering

Simon Herbinger, Biome Renewables Inc.

Davide De Cicco, Dalhousie University

Sahra Skripsky, Dalhousie University

Ryan Church, Biome Renewables Inc.

Abstract

Biome Renewables Inc. in collaboration with Glas Ocean Engineering, Alison Mark Consulting, Researchers from Dalhousie University and Queen's University Belfast (QUB), completed an analysis of the PowerCone as a tidal current turbine and investigated new materials for use in tidal turbines. The project consisted of a comparison of the performance of a horizontal axis tidal turbine from QUB that is 1.5m in diameter. The turbine was tested with different blade configurations and with and without the PowerCone and the new material blades: Fiber Metal Laminate Material (FML). The performance and resistance to impact of FML blades was measured as well as the performance of the turbine with a PowerCone attachment and the performance of a full PowerCone turbine. A $1/10^{th}$ scale Schottel tidal turbine was on loan from Queen's University Belfast as well as their traditional 4 blade tidal turbine. The testing was completed in a controlled laboratory environment using a 300 m^3 rectangular ballast tank located in the Aquatron Laboratory of Dalhousie University. The electrical power output at a range of rpm was plotted to compare the performance of each configuration tested. Results indicated that the PowerCone produced higher quality power curves than the original turbine blades alone in the energetic flow. Initial review of the acquired data shows that the PowerCone has promise as a tidal turbine and in particular in highly turbulent and shallow sites. It is recommended that further testing be completed in a testing site such as the QUB site in Strangford Lough.

Table of Contents

Abstract ii

List of Figures iv

List of Tables v

Introduction 1

Experimental setup 3

Frame 3

Turbine 4

Tank 5

Crate 6

Turbine in tank setup 7

Test Plan 9

PowerCone 9

M-hub 10

Fiber Metal Laminate Blades 12

Tests 13

Experimental procedure 14

Testing 14

3 Schottel hub, comparing CCW and CW performance 15

4 Eppler hub 16

FML Blade fabrication 17

4 FML hub 17

4 FML hub blade impact test 18

3 Schottel hub PCone 18

3 Eppler hub, comparing performance with and without M-hub (angled blades) and PowerCone 19

Control Systems 21

Post Processing 22

Test Results 23

3 Schottel hub performance in different rotation directions 23

4 FML hub 27

3 Schottel hub without and with PowerCone 27

3 Eppler hub or M-hub with and without PowerCone 29

Thrust loads 32

Comparison of Configurations – Mechanical Power....35
Discussion....36
Conclusion....40
References....42

List of Figures

Figure 1: Assembly of turbine support frame....3
Figure 2: 1/10 scaled tidal turbine (Jeffcoate et al. 2016)....4
Figure 3: Ballast tank used for testing....5
Figure 4: Steel frame setup with Vector....6
Figure 5: Frame and cinder block set....6
Figure 6: Turbine in crate....7
Figure 7 Turbine being lifted out of crate....8
Figure 8 Turbine being lowered into tank....8
Figure 9 Turbine being attached to frame....8
Figure 10 Turbine in tank....8
Figure 11 Turbine in Tank....8
Figure 12: Ceramic PowerCone fixed with epoxy and fiberglass....10
Figure 13: Larger Powercone on Turbine body....11
Figure 14 Smaller Powercone on Schottel hub exploded view....11
Figure 15 Powercone on Schottel hub....11
Figure 16 Powercone on M-hub....11
Figure 17 Powercone on M-hub exploded view....11
Figure 18 Powercone on M-hub....12
Figure 19 Powercone on M-hub exploded view....12
Figure 20: Turbine in tank experimental setup....12
Figure 21: FML blades....14
Figure 22: Set up of the three Schottel Hydro SIT250 scaled blades (3 Schottel hub)....15
Figure 23: **Left**: Turbine stopped rotating, nosecone and hub are bent downwards. **Right**: Rotor collars, damaged collar to the right, new replacement collar to the left....16
Figure 24: The four Eppler E387 blade hub (4 Eppler hub), **Left**: not installed and **Right**: installed on the turbine in the tank....16
Figure 25: The 4 Fiber Metal Laminate blade hub installed on the turbine and **Far right**: with accelerometer mounted on the blade....18
Figure 26: Wooden impact test stick....18
Figure 27: **Left**: 3 Schottel hub without blades**. Right**: Ceramic PowerCone on 3 Schottel hub....19
Figure 28: 3 Eppler blade hub **Left**: on the turbine and **Right**: unmounted. Here the blades are perpendicular to the turbine axis....20
Figure 29: **Left**: 3 Eppler M-hub, with blades angled back (no nosecone). **Right**: 3 Eppler M-hub, with blades angled back, with PowerCone....20
Figure 30: Schematic of the tidal turbine closed-loop Proportional-Integral-Derivative (PID) control system,and programmable load system from Frost et al. 2018....22

Figure 31: Mechanical Power vs RPM for 3 Schottel hub rotating CCW 24
Figure 32: Coefficient of electrical power vs tip speed ratio for 3 Schottel hub rotating CCW 24
Figure 33 Mechanical power for 3 Schottel hub rotating CCW compared with CW. 25
Figure 34 Coefficient of electrical power for 3 Schottel hub rotating CCW compared with CW. 25
Figure 35 Mechanical Power vs RPM for 3 Schottel hub CW with blade at 12˚ 26
Figure 36 Mechanical Power vs RPM for 3 Schottel hub CW with blade at 24 26
Figure 37 Mechanical power vs RPM for 4 FML hub 27
Figure 38 Mechanical Power vs RPM for 3 Schottel hub with PowerCone 28
Figure 39 Mechanical power vs RPM for 3 Schottel hub with and without PowerCone 28
Figure 40 Mechanical power vs RPM for 3 Eppler hub 29
Figure 41 Mechanical power vs RPM for the 3 Eppler M-hub no PowerCone 30
Figure 42 Mechanical power vs RPM for the 3 Eppler M-hub PCone 30
Figure 43 Mechanical power per swept area as a function of RPM for 3 Eppler M-hub with and without PowerCone and 3 Eppler hub 31
Figure 44 Mechanical power vs RPM for 3 Eppler M-hub with and without the PowerCone 32
Figure 45 Thrust for 3 Schottel hub rotating CW and CCW 33
Figure 46 Thrust for 3 Schottel hub with and without PowerCone 33
Figure 47 Thrust for 3 Eppler hub and 3 Eppler M-hub with and without PowerCone 34
Figure 48 Mechanical Power versus Flow velocity for a number of configurations 35

List of Tables

Table 1 Test Matrix 9
Table 2 Test configurations 14
Table 3 Test runs to compare Schottel CCW and CW performance 15
Table 4 Test run to measure 4 Eppler hub performance 17
Table 5 Tests run to measure 4 FML hub performance 17
Table 6 Tests run to measure 3 Schottel hub PCone performance 19
Table 7 Tests run to compare 3 Eppler hub performance with and without M-hub (angled blades) and PowerCone. 21

Introduction

Tidal power offers communities an attractive opportunity for predictable renewable energy. In combination with energy storage, tidal power can act as a base load and ease the transition to fossil free power generation.

Nova Scotia is known for having the highest tides and strongest currents in the world (Garrett, 1972) and the work being done by companies and researchers in the Bay of Fundy is building expertise and experience that can be exported around the world. Developers in the Bay of Fundy are building systems to withstand an average flow of 5m/s. Globally, however the majority of tidal sites average 1.8-2m/s. Building on the knowledge gained in Nova Scotia it is possible to design efficient systems that can be used in lower speed sites.

Biome Renewables have developed a retrofit for wind turbines, the PowerCone, that increases the efficiency of the systems and increases the annual energy production (AEP) by 13% (https://www.biome-renewables.com/powercone). The PowerCone also improves performance in uneven flow and lowers cut-in speed. This project was designed to evaluate the PowerCone in tidal flow and determine if it was likely to offer similar benefits. Similar performance improvements in tidal turbines would mean the PowerCone could increase the AEP from high speed sites such as those in the Bay of Fundy or the Pentland Firth and it would also increase the number of lower speed locations globally where tidal turbines can be used economically.

Tidal or hydrokinetic turbines operate in channels, rivers and high flow sites that are often subject to significant erosion. The potential for blades to suffer impact from material such as stones or branches at high speed is very high and the material the turbines are fabricated from is of particular interest to technology developers. Dr. Farid Taheri and his research group at Dalhousie University have developed a novel 3D composite material that (i) is relatively light-weight, (ii) has excellent stiffness and strength (iii) offers remarkable impact strength and (iv) yet is economical. The new material takes advantages of a marriage of a light-weight metallic alloy and a relatively inexpensive 3D E-glass fabric as an effective approach to reach the targeted goals. The resulting material is referred to as fiber-metal-laminates (FML). While 2D FML has been used in several aircraft since the 90s, the developed material is the first 3D rendition of FML.

It is believed that the exemplary high specific-stiffness and weight of this material make it a serious contender for application in turbines, in the format of blades, in both submerged and wind turbines. However, before this FML can be used in such applications, one must gain a thorough understanding of its performance under critical loading conditions that such structural components would encounter. This project, therefore, aims at characterizing the performance of the material under critical conditions that a submerged turbine encounters.

The PowerCone and FML testing were completed in the same test series which allowed the Biome and Dalhousie teams to more economically investigate performance. Using the turbine from Queens University Belfast (QUB), the team had a platform for testing the PowerCone in a number of configurations and the FML material was evaluated through testing of a blade constructed of the FML material with an embedded vibration sensor. The goal of this research project was to gain comparable results to those acquired in previous testing environments to determine the performance of the turbine with different blade configurations in a 300 m^3 rectangular ballast tank, the performance and resistance to impact of FML (fiber metal laminate) material for the blades, and the performance of the turbine with a PowerCone nose attachment that was designed by Biome Renewables.

The $1/10^{th}$ scale Schottel tidal turbine blades used for this testing were on loan from Queen's University and there are numerous studies published on this same turbine. Jeffcoate et al. (2016) explored the performance of this turbine using pushing tests conducted at a field site in Strangford Narrows, Northern Ireland. Frost et al. (2017) presented and compared data from two experimental tests done at CNR-INSEAN's towing tank in Italy and the Strangford Lough tidal test site in Northern Ireland, to address the knowledge gap between laboratory and in-situ testing with this tidal turbine.

For this research project, Dr. Sue Molloy, Dr. Aaron MacNeil, Dr. Farid Taheri, Davide De Cicco and Dr. Alison Mark, all researchers in Halifax, worked along with Ryan Church, CEO of Biome Renewables and interns Simon Herbinger and Sahra Skripsky. Dr. Carwyn Frost of QUB was available for advice throughout the project.

Experimental setup

This was the first installation of this turbine in the Aquatron ballast tank. It was also the first time that this particular Aquatron tank was used for turbine testing. The ballast tank was chosen over the big tank for the potential speed of the flow and the workspace and this required construction of a frame, characterisation of the water flow and evaluation of the turbine performance compared to previous test sites.

Frame

The team designed a frame system that would hold the turbine in place over the tank for testing. The following constraints were taken into consideration during the design process:

- the frame should be strong enough to support the entire weight of the turbine and resist vibrations from the flow,
- the frame should be free to move to change its position over the length of the tank and the cost of the materials, parts and assembling should be within the $2000 budget.

After several design iterations, it was decided to use two steel H-beams to create a T-shaped frame with caster wheels.

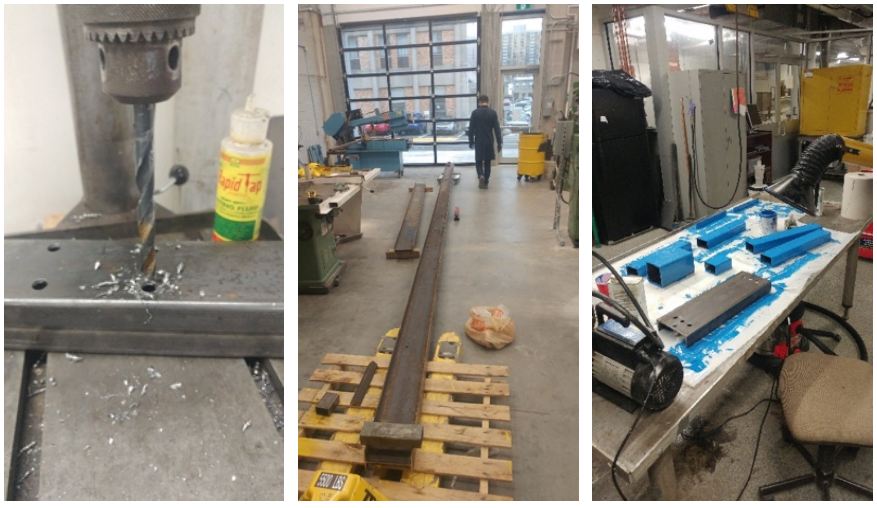

Figure 1: Assembly of turbine support frame

Assembly was completed on site at Dalhousie University. Three rectangular steel tubes were used to attach the top of the turbine to the beams and several angle beams provided a connection at the

top of the frame and stoppers at the ends. The frame was then covered with an anti-corrosive paint and assembled on top of the ballast tank (Figure 1).

Turbine

The tidal turbine has a diameter of 1.5 m, is 2.52 m from the top plate to the bottom of the nacelle and has a mass of 363 kg (Jeffcoaste et al. 2016) (Figure 2). The turbine is set up to accommodate both 3-blade and 4-blade rotors. The blades for the 4-blade rotor have Eppler E387 airfoil geometry, each blade is 0.575 m long, with a root pitch angle of 32° (Frost et al, 2018). The Eppler blades can also be attached to a three-blade rotor. Another set of available blades for a three-blade rotor are scaled Schottel Hydro SIT250 blades (Frost et al. 2017). The thrust loading sensor is in the housing of the turbine (Frost et al. 2018). There are sensors behind the rotor, providing torque (T, Nm) and rotational velocity (ω, rad.s^{-1}) (Frost et al. 2017). The power from the generator signals are recorded by the data acquisition (DAQ) box located above the water surface along with the power regulators and dissipaters (Frost et al. 2017).

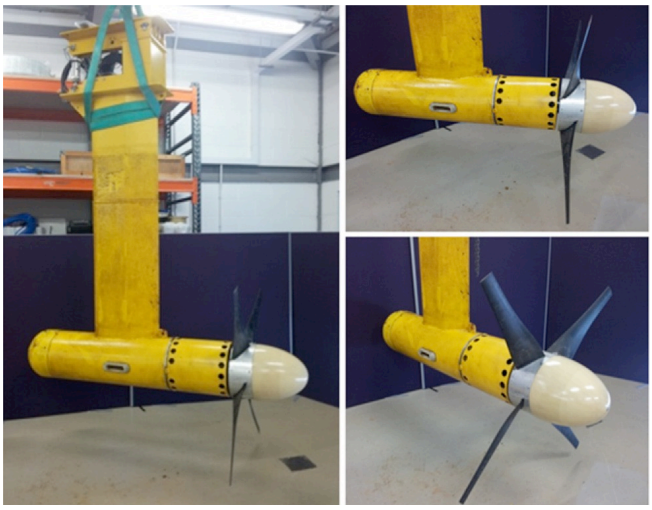

Figure 2: 1/10 scaled tidal turbine (Jeffcoate et al. 2016)

Tank

The ballast tank had not been previously used for turbine testing and it was important to understand the type of flow to which the turbine would be exposed. The inlet pipes in the tank were closer to the surface of the water than the level of the blades. Several considerations for redirecting the flow onto the turbine blades were explored. Richard Cheel of Dalhousie assisted the team in understanding the flow through an analysis with an Acoustic Doppler Current Profiler (ADCP). The flow was determined to be very turbulent with significant spatial variation. It was also determined to be sensitive to the control inputs for the flow such as pump power percentage and the fraction that the inlet valves were closed. After discussion and analysis, it was agreed to not implement a flow redirector and leave the inlets as is.

The rectangular pool tank is 300 m^3 in volume, 9.1 m long, 7.3 m wide, and 4.5 m deep, and filled with unfiltered seawater (Dalhousie University, Aquatron Laboratory, Figure 3).

Figure 3: Ballast tank used for testing

The corners of the tank are chamfered to help reduce water flow dead spots within the tank (Dalhousie University, Aquatron Laboratory). During all testing, the first pipe inlet was fully closed, the second inlet was closed by 1.25 notches, and the third inlet was fully opened. To allow better turbine placement after the frame was fabricated, it was raised ~40 inches by five concrete blocks (16-inch x 8-inch x 10-inch) at each endpoint of the T and the caster wheels were removed (Figure 4). It was stabilized with two threaded rods that were grounded by concrete drop-in anchors

drilled into the top walls of tank (Figure 5). The water level was decreased to 0.49 m from the top of the tank wall so that the turbine was submerged by 0.903 m.

Figure 4: Steel frame setup with Vector

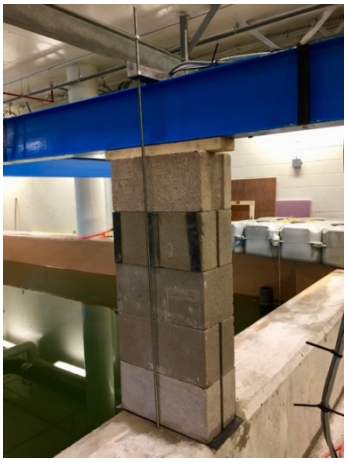

Figure 5: Frame and cinder block set

Crate

The crate shipped from QUB containing the turbine and necessary testing equipment was received at Dalhousie University January 16th (Figure 6).

Figure 6: Turbine in crate

Turbine in tank setup

QUB researchers Carwyn Frost and Ian Beson visited Halifax to assist in setting up the turbine and control systems for testing. Using an overhead crane, the turbine was moved above the pool tank (Figure 7 & Figure 8). The pivot plate which is connected to the turbine strut, was then connected to the center of the T-shaped frame (Figure 9). This pivot plate allowed the turbine to be lifted and lowered and connectors fixed the turbine in position (Figure 10 & Figure 11). The pivot plate also has a turnbuckle that transfers the horizontal loading of the turbine to a load pin (Jeffcoate et al. 2016). The flow in the tank was mapped again with a Nortek velocimeter (Vector) that was moved to three different positions along the length and breadth of the tank. By mapping out the flow at nine different locations in the tank, the researchers were able to determine the best position to place the turbine for testing. The tank velocity was measured using a Nortek Aquadopp ADP which was mounted to the centre of the steel frame, 1.26 m out from the frame.

Figure 7 Turbine being lifted out of crate

Figure 9 Turbine being attached to frame

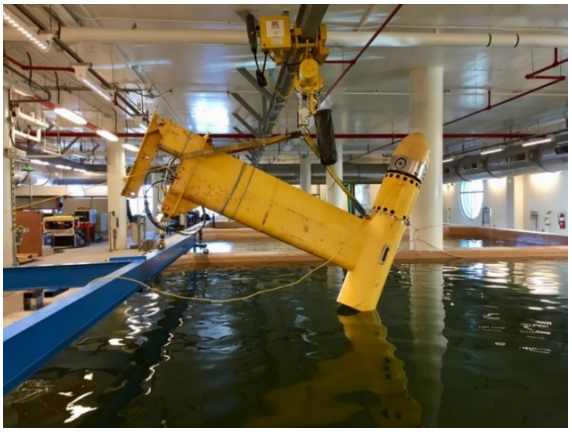

Figure 8 Turbine being lowered into tank

Figure 10 Turbine in tank

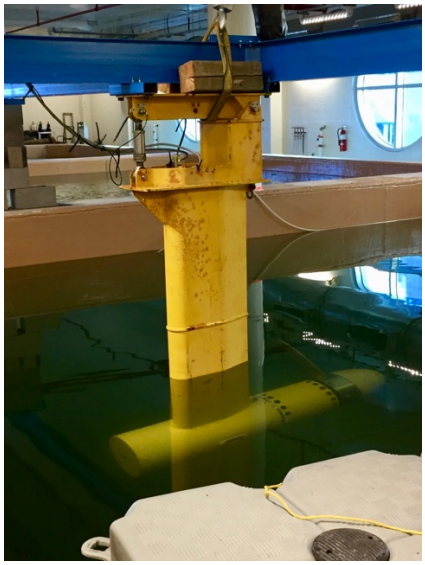

Figure 11 Turbine in Tank

Test Plan

Testing of several different blade configurations was planned and with limited time available in the tank, effort was made to plan the testing efficiently. Papers published that referenced this turbine (Jeffcoate et al. 2016, and Frost et al. 2018) were used as references in plan development. Considerations included changeouts of different configurations and fabrication of components. The water in the tank needed to be lowered for every changeout.

Table 1 Test Matrix

Test	Configuration	Measured	Note
1a	3 Schottel blades	Torque, RPM, V, I, Thrust	Turbine/blade performance data for comparison to previous test results, baseline for PowerCone performance tests
1b	4 Eppler blades	Torque, RPM, V, I, Thrust	Turbine/blade performance data for comparison to previous test results
1c	3 Eppler blades	Torque, RPM, V, I, Thrust	Turbine/blade performance data for baseline for PowerCone performance tests
2a	3 Schottel blades with PowerCone	Torque, RPM, V, I, Thrust	PowerCone performance data
2b	3 Eppler with M-hub (angled blades)	Torque, RPM, V, I, Thrust	M-hub performance data and baseline for PowerCone performance tests
2c	3 Eppler with M-hub with PowerCone	Torque, RPM, V, I, Thrust	PowerCone performance data
3a	4 FML blades	Torque, RPM, V, I, Thrust, Vibration	Blade performance data, blade material performance data
3b	4 FML blades under impact	Torque, RPM, V, I, Thrust, Vibration	Blade material performance data

PowerCone

The Biome Renewables product, the PowerCone, is inspired by bio-mimicry and is currently a retrofit for traditional nosecones on wind turbines as described above. An SLA 3D printed ceramic

PowerCone created for previous wind turbine testing with Biome Renewables was damaged in transit and repaired with epoxy and fiberglass (Figure 12).

Figure 12: Ceramic PowerCone fixed with epoxy and fiberglass

M-hub

It was postulated that a large PowerCone in place of the nose cone and turbine blades could perform well. In order to examine this an approximation of a large PowerCone style turbine was built by changing the orientation of the existing blades to align with the PowerCone nosecone blades. The small PowerCone was combined with the Eppler blades fixed at a 60° angle backwards from the axis of rotation to simulate a larger PowerCone. This new approach was named the modified-hub or m-hub as a new hub design was used to orient the blades. Designs that were considered are in Figure 13 to Figure 19.

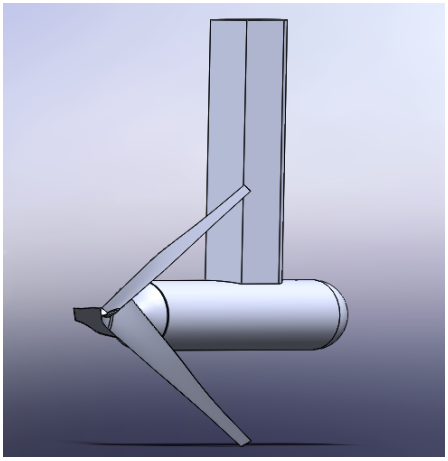

Figure 13: Larger Powercone on Turbine body

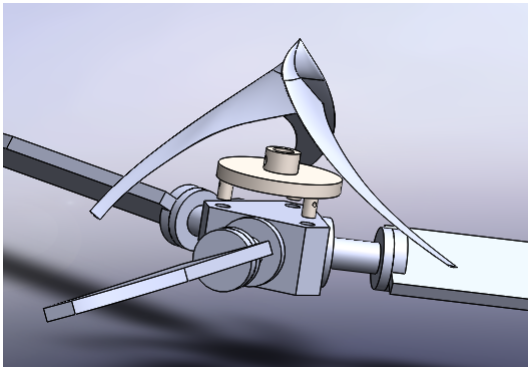

Figure 14 Smaller Powercone on Schottel hub exploded view

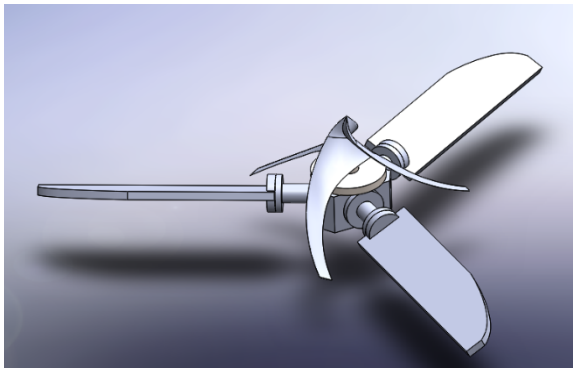

Figure 15 Powercone on Schottel hub

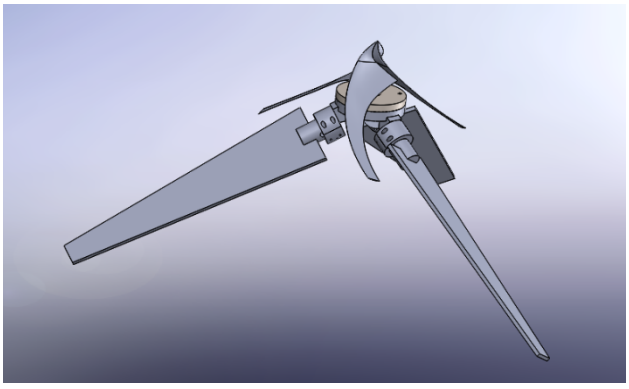

Figure 16 Powercone on M-hub

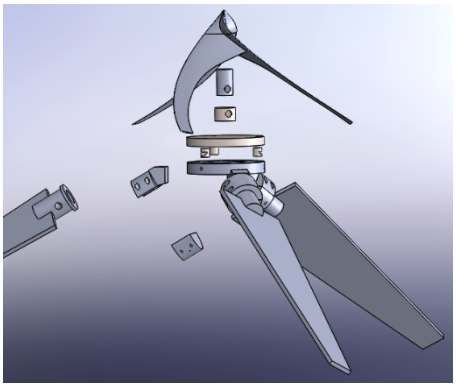

Figure 17 Powercone on M-hub exploded view

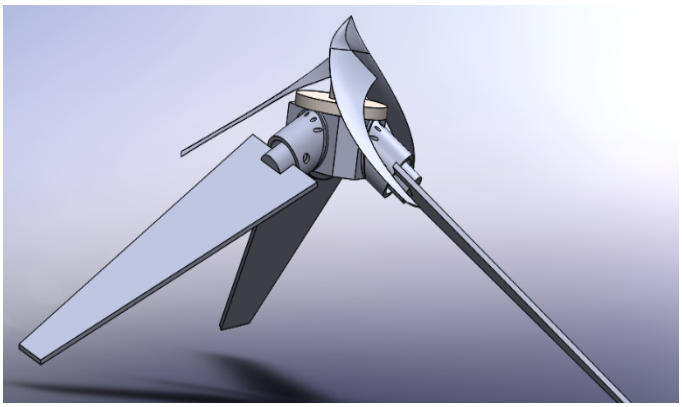

Figure 19 Powercone on M-hub

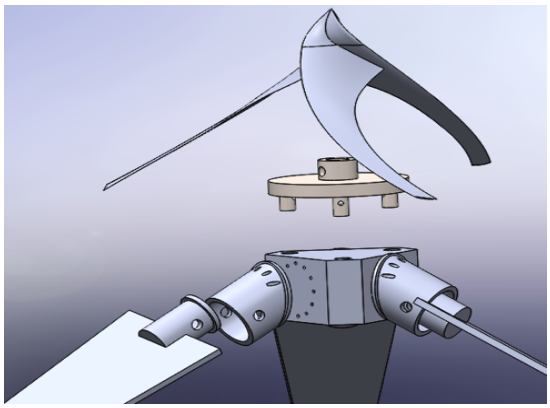

Figure 18 Powercone on M-hub exploded view

Figure 20: Turbine in tank experimental setup

Fiber Metal Laminate Blades

A set of turbine blades was fabricated using the fiber metal laminate material (FML) (Figure 21). This material is lightweight, very stiff and has a low production cost.

Fibre metal laminates (FMLs) form a family of composite materials that have been in development for some time. A common example is GLARE (glass laminate aluminum reinforced epoxy), which consists of layers of thin aluminum and E-glass prepreg, interspersed. FMLs are most commonly used in the aircraft industry and have been shown to have excellent impact resistance and fatigue

performance, and greater specific strength and stiffness than the fibre reinforced polymers (FRPs) they usually replace [Asaee, 2015] They are also significantly more formable [Asaee, 2017].

FMLs with magnesium are much less common, but some studies have been done; these show that the specific impact energy of magnesium FMLs is similar to that of aluminum FMLs. Magnesium has advantages in lower density and cost [DeCicco, 2017].

3DFMLs were developed to build on the success of FMLs. In these, the core of the sandwich is a 3D fibre-glass fabric consisting of two bi-directional weave fabric layers with vertical braided glass fibre pillars between them. Tests performed in Dr. Taheri's lab at Dalhousie showed that the 3DFMLs absorbed higher impact energy and showed less damage compared to FMLs. The 3DFMLs also had the highest specific flexural stiffness of a group of samples, including several thicknesses of FMLs [Asaee, 2015].

The most recent development in these materials has been the addition of amino-functionalized graphene nanoparticles (GNPs) to the resin adhering the various layers together. Dr. Taheri's team saw, with the correct amount of GNPs, improvements in impact response (greater energy absorption and less damage) and in ductility of 3DFMLs [Asaee, 2017].

The low weight, good strength and high specific stiffness of the new 3DFML material suggested applications in turbine blades. The excellent impact performance would seem to make a 3DFML blade resilient; however, its behaviour in real world environments, particularly in water, was untested. This study was a first step in addressing that lack.

We hypothesised that this blade material could lead to a) better turbine function because there would be more energy extraction for a given flow rate, and b) longer blade life, which would lead to more energy extraction over time because there would be fewer maintenance periods for blade replacement. The 'reliability and the survivability' of the blades would improve.

Tests

The goal for the blade testing in this project was to test the industrial application of this material for turbine blades, in water and in wind. In tests with this set of blades the vibrational response of the blades was measured using an accelerometer in addition to measuring the turbine performance metrics.

Figure 21: FML blades

Experimental procedure

Testing

Different blade configurations were tested at a range of RPM values to compare performances. The blade configurations are described in Table 2.

Table 2 Test configurations

Configuration	Blades	Rotation Direction	PowerCone or M-hub	Test Date
3 Schottel hub, CCW	Schottel Hydro SIT250 scaled	CCW	-	25 March
3 Schottel hub	Schottel Hydro SIT250 scaled	CW	-	1, 2 April
3 Schottel PCone	Schottel Hydro SIT250 scaled	CW	PowerCone	2 April
3 Eppler hub	Eppler E387	CW	-	3 April
3 Eppler M-hub	Eppler E387	CW	M-hub	4 April
3 Eppler PCone	Eppler E387	CW	M-hub + PowerCone	5 April
4 Eppler hub	Eppler E387	CW	-	
4 FML hub	Fibre Metal Laminate	CCW	-	1 April

3 Schottel hub, comparing CCW and CW performance

The first run with the 3 Schottel hub (Figure 22). There was high variation in the RPM mainly driven by turbulence. The turbine had no load regulator connected for this test. The turbine depth was estimated to be 1.3m below the surface and it was rotating CCW. The depth of water was reduced, leaving the turbine at 0.9 m below the water's surface. The PID parameters were set to P = 1.5, I = 0.003, D = 0.003.

The 3 Schottel hub was tested several times running CCW, its design direction, and then running CW, as it would be run with the PowerCone. A baseline measurement of the CW Schottel performance would be required for the later PowerCone performance assessment. The details of the various tests are given in Table 2.

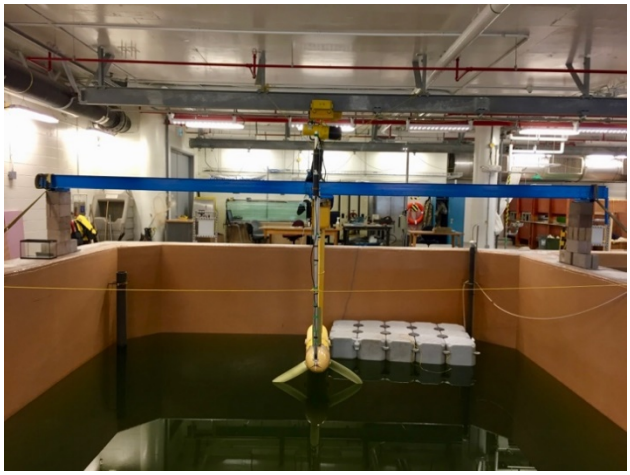

Figure 22: Set up of the three Schottel Hydro SIT250 scaled blades (3 Schottel hub).

Table 3 Test runs to compare Schottel CCW and CW performance

Configuration	Rotation direction	RPM values (incr. 10 default)	Pump power	Duration of data collection
3 Schottel hub	CCW	-10 to -110 (x3)	80%	600s
3 Schottel hub	CCW	-10 to -110 (x2)	85%	600s
3 Schottel hub	CCW	-20 to -90	80%	600s
3 Schottel hub*	CW	50 to 90	80%	900s
3 Schottel hub	CW	50 to 90	80%	900s
3 Schottel hub	CW	10, 15, 20	80%	600s
3 Schottel hub	CW	15, 20, 30	90%	600s
3 Schottel hub	CW	10 to 30 (incr. 5)	70%	600s

* After this test run the blade pitch angle was changed (from 12° to 24°)

In the last round of CCW tests at 85% power the hub stopped rotating when the RPM was changed from -70 to -40. This was due to corrosion of the rotor collar (Figure 23). The rotor collar was replaced with a new replacement part and testing was resumed.

*Figure 23: **Left**: Turbine stopped rotating, nosecone and hub are bent downwards. **Right**: Rotor collars, damaged collar to the right, new replacement collar to the left.*

The 3 Schottel hub rotating CW was tested in two sessions. Halfway through the first session, the blade pitch of the Schottel blades was changed. During the second session, the nosecone fell off ~340 seconds into testing at 15 RPM at 80% pump power and was not reattached.

4 Eppler hub

The 4 Eppler hub (Figure 24) was tested; details are given in Table 4. During testing there were periods when rotation was stalled.

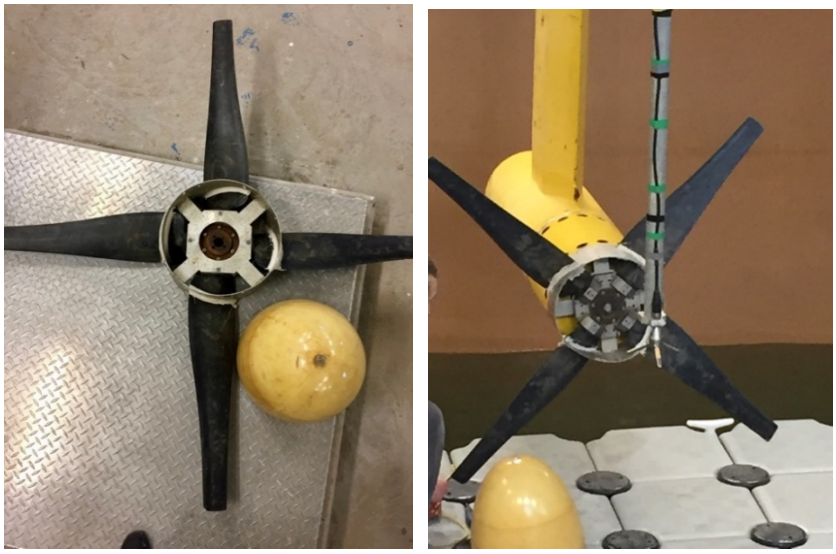

*Figure 24: The four Eppler E387 blade hub (4 Eppler hub), **Left**: not installed and **Right**: installed on the turbine in the tank.*

Table 4 Test run to measure 4 Eppler hub performance

Configuration	Rotation direction	RPM values (incr. 10 default)	Pump power	Duration of data collection
4 Eppler hub	CW	20 to 100	80%	600s

FML Blade fabrication

The blades were fabricated in Dr. Taheri's materials lab at Dalhousie University.

The first stage was to stiffen the 3D fabric (10 mm thickness [Asaee, 2016]); for this, epoxy resin and hardener were mixed and degassed, applied to the fabric, and cured in an oven (2 hours at 60°C then 8 hours at 120°C). Next the hollows in the 3D fabric were filled using a two-part polyurethane foam, injected by syringe and allowed to cure.

The second stage was to mix the GNPs into the resin for bonding the sandwich. The same resin system was used; this time GNPs were added to the resin, the mixture was stirred with an electric mixer and then passed through a 3-roll mill. Then the hardener was added and the mixture was degassed.

The third stage was to prepare the magnesium sheets. The surfaces were sand-blasted, then cleaned with compressed air and acetone.

Finally, the sandwich was assembled using the GNP enhanced epoxy, the whole thing was vacuum-bagged and cured following the same temperature profile as in stage one [Asaee, 2017].

Once the blade had fully cured, rubber edging was wrapped around the edges and bonded to the blade sandwich to seal the 3D fabric; then whole blade was coated with white spray paint.

4 FML hub

The 4 FML hub was installed (Figure 25) and tested with the parameters given in Table 5. An accelerometer was attached to one of the blades during testing. On the second day, ~446 seconds into testing at -100 RPM the nosecone came off of the turbine and was not reattached. At the start of testing on the third day, the nosecone was reattached to the hub; however ~550 seconds into testing at -40 RPM the nosecone came off again and was not reattached.

Table 5 Tests run to measure 4 FML hub performance

Configuration	Rotation direction	RPM values (incr. 10 default)	Pump power	Duration of data collection
4 FML hub	CCW	-20	80%	600s
4 FML hub	CCW	-20, -30, -100	80%	600s
4 FML hub	CCW	-20 to -40 (incr. 5)	80%	600s

*Figure 25: The 4 Fiber Metal Laminate blade hub installed on the turbine and **Far right**: with accelerometer mounted on the blade.*

4 FML hub blade impact test

The impact test on the FML blades was done with the RPM set to -40 and 80% pump power. The wooden stick (Figure 26) impacted the blades repeatedly for 5 minutes.

Figure 26: Wooden impact test stick

3 Schottel hub PCone

The ceramic PowerCone was attached to the 3 Schottel hub (Figure 27) and then mounted on the turbine. Tests were carried out as given in Table 6.

Table 6 Tests run to measure 3 Schottel hub PCone performance

Configuration	Rotation direction	RPM values (incr. 10 default)	Pump power	Duration of data collection
3 Schottel hub PCone	CW	10 to 30 (incr. 5)	70%	600s
3 Schottel hub PCone	CW	10 to 30 (incr. 5)	80%	600s
3 Schottel hub PCone	CW	10 to 30 (incr. 5)	90%	600s

*Figure 27: **Left**: 3 Schottel hub without blades. **Right**: Ceramic PowerCone on 3 Schottel hub.*

3 Eppler hub, comparing performance with and without M-hub (angled blades) and PowerCone

The 3 Eppler hub with perpendicular blades was installed (Figure 28). Baseline testing was done with no nosecone, using the parameters given in

Table *7*. The Eppler blades were then moved to the M-hub where the blades were angled back toward the turbine (Figure 29). This configuration was then tested. Finally, the PowerCone was mounted on the front of the M-hub (Figure 29) and the whole package was tested. Test parameters are given in

Table *7*.

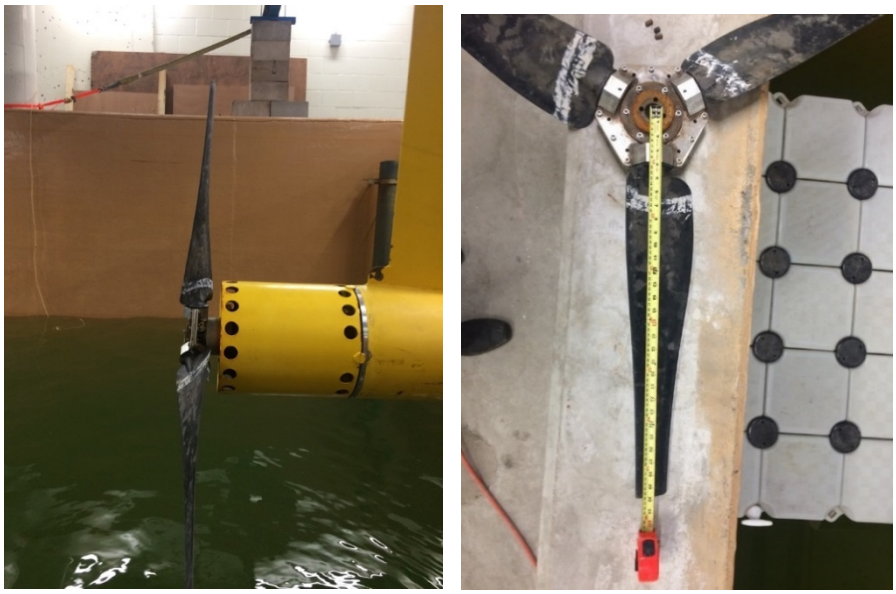

*Figure 28: 3 Eppler blade hub **Left**: on the turbine and **Right**: unmounted. Here the blades are perpendicular to the turbine axis.*

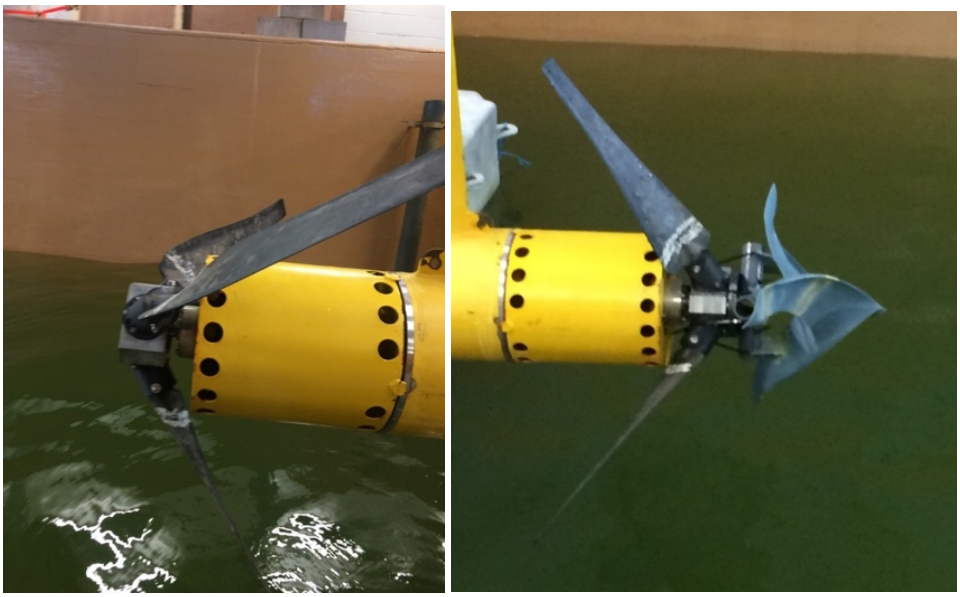

*Figure 29: **Left**: 3 Eppler M-hub, with blades angled back (no nosecone). **Right**: 3 Eppler M-hub, with blades angled back, with PowerCone.*

Table 7 Tests run to compare 3 Eppler hub performance with and without M-hub (angled blades) and PowerCone.

Configuration	Rotation direction	RPM values (incr. 10 default)	Pump power	Duration of data collection
3 Eppler hub	CW	10 to 30 (incr. 5)	70%	600s
3 Eppler hub	CW	10 to 30 (incr. 5)	80%	600s
3 Eppler hub	CW	10 to 30 (incr. 5)	90%	600s
3 Eppler hub*	CW	20 to 40 (incr. 5)	80%	60s
3 Eppler M-hub	CW	10 to 30 (incr. 5)	70%	600s
3 Eppler M-hub	CW	10 to 30 (incr. 5)	80%	600s
3 Eppler M-hub	CW	10 to 30 (incr. 5)	90%	600s
3 Eppler M-hub*	CW	20 to 40 (incr. 5)	80%	60s
3 Eppler M-hub PCone	CW	10 to 30 (incr. 5)	70%	600s
3 Eppler M-hub PCone	CW	10 to 30 (incr. 5)	80%	600s
3 Eppler M-hub PCone	CW	10 to 30 (incr. 5)	90%	600s

* With accelerometer mounted on one blade.

Control Systems

The tank was filled and drained via a web-based control system, the Aquatron Tidal Flow System, which also controlled the water flow rate (Dalhousie University, Aquatron Laboratory). This software allows the user to select the power level of each of the four pumps and the number of pumps used to produce the flow (MacNeill et al. 2017).

The tidal turbine used in this study features a closed-loop Proportional-Integral-Derivation (PID) controller programmed to maintain a constant RPM; the PID control system ran as a virtual instrument though the program LabView in the Data Acquisition (DAQ) programme (Frost et al. 2017, Frost et al. 2018, Figure 30). To control the turbine, a set RPM was chosen, and the system would attempt to maintain that speed whatever the water flow speed. The proportional constant, P(Kc), or gain, was set to either a positive or negative value, depending on the rotational direction

of the driveshaft (Frost et al. 2018). When the driveshaft rotated clockwise the P(Kc) was set to -1.5 and while when the driveshaft rotated counter clockwise, the P(Kc) was set to 1.5. For the testing done in this paper, both the integration time constant (Ti) and the differential time constant (Td) had set values of 0.003 min.

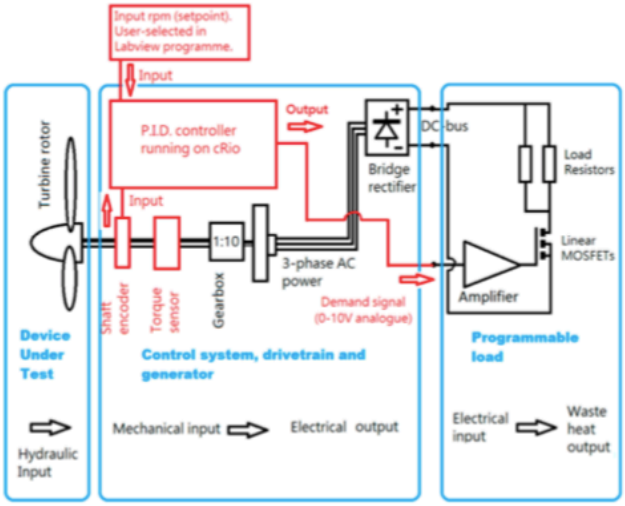

Figure 30: Schematic of the tidal turbine closed-loop Proportional-Integral-Derivative (PID) control system,and programmable load system from Frost et al. 2018.

Post Processing

The mechanical and electrical power produced by the turbine, the power coefficient, Cp, and the tip speed ratio, TSR or λ, were calculated for the various turbine configurations.

The mechanical power, P_{mech}, generated by the turbine was calculated using the torque, τ, and the revolutions per minute (RPM), n (Jeffcoate et al. 2016);

$$P_{mech} = \tau \frac{2\pi n}{60}$$

The electrical power, P_{elec}, from the generator was calculated using voltage, V, and current, I, measurements collected by the data acquisition box (Jeffcoate et al. 2016);

$$P_{elec} = V * I$$

The power available in the flow, P_{flow}, over the swept area of the rotor, A, was calculated where ρ is the water density ($1000\ kg/m^3$) and U is the depth-averaged, time-averaged flow velocity (Jeffcoate et al. 2016):

$$P_{flow} = \frac{1}{2}\rho A U^3$$

The mechanical power coefficient ($C_{p(mech)}$)is the fraction of the power available in the flow (P_{flow}) that is extracted by the turbine (P_{mech}) (Jeffcoate et al. 2016):

$$C_{p(mech)} = \frac{P_{mech}}{P_{flow}}$$

The electrical power coefficient ($C_{p(elec)}$) was also calculated;

$$C_{p(elec)} = \frac{P_{elec}}{P_{flow}}$$

The tip speed ratio, λ or TSR, is determined using the rotor radius, R, the rotational velocity, ω, in rad/s, and the inflow velocity (Jeffcoate et al. 2016);

$$\lambda = \frac{R\omega}{U}$$

The power curve (C_p *vs.* λ) for tidal turbines is expected to resemble a bell curve. The relationship between mechanical power and rotational speed (RPM) is generally close to linear.

Test Results

3 Schottel hub performance in different rotation directions

The Schottel hub and blades were initially tested rotating CCW, as they were designed to run. A torque sensor measured the torque experienced by the turbine and a tachometer was used to measure the rotational speed of the turbine. This data was used to calculate mechanical power and plot its relationship with RPM (Figure 31). The power curve using $C_{p(elec)}$ for this blade configuration was determined and is presented in Figure 32. Scatter in the plots is attributed to both noise and variation due to turbulence in the flow.

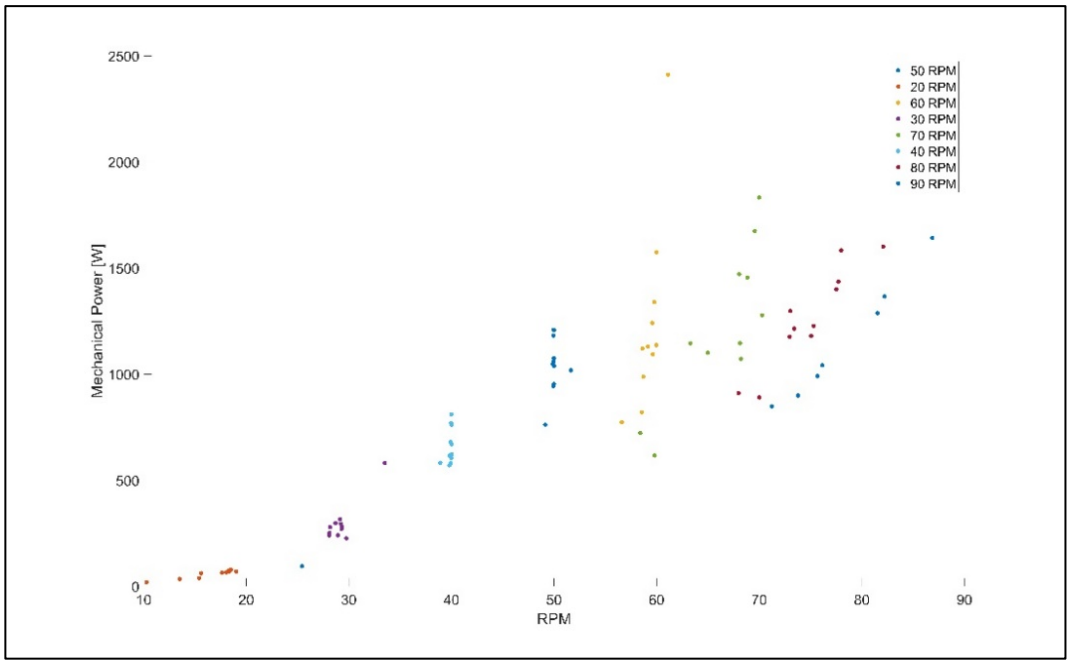

Figure 31: Mechanical Power vs RPM for 3 Schottel hub rotating CCW

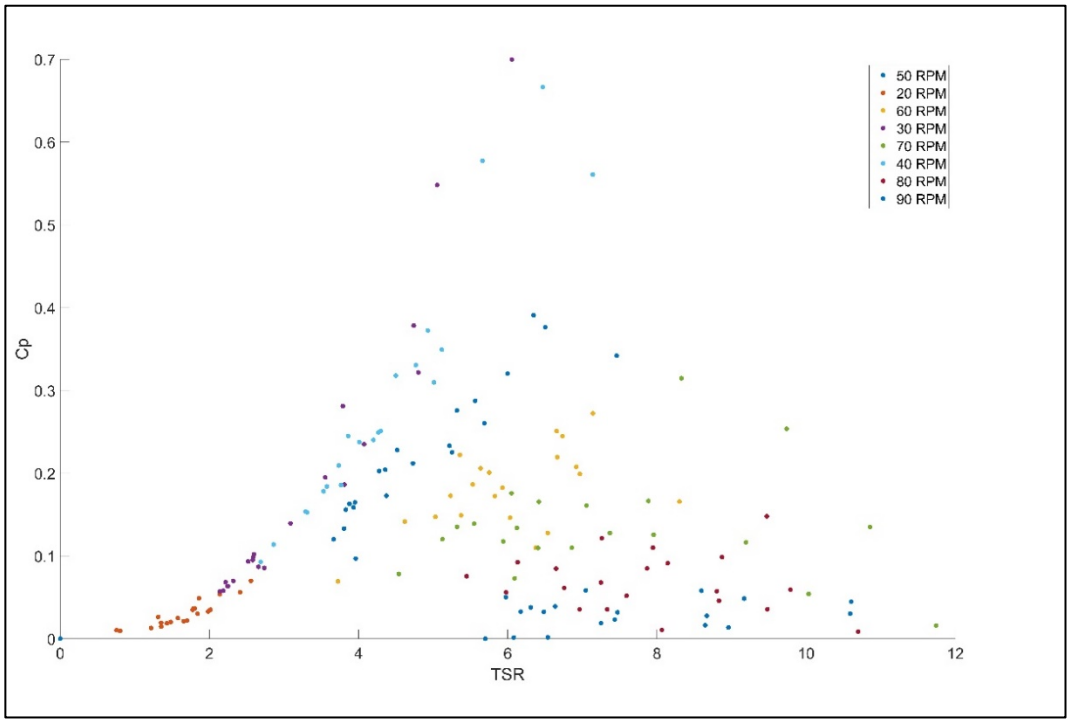

Figure 32: Coefficient of electrical power vs tip speed ratio for 3 Schottel hub rotating CCW

The performance of the 3 Schottel hub in both CCW and CW directions is presented in Figure 33 and Figure 34.

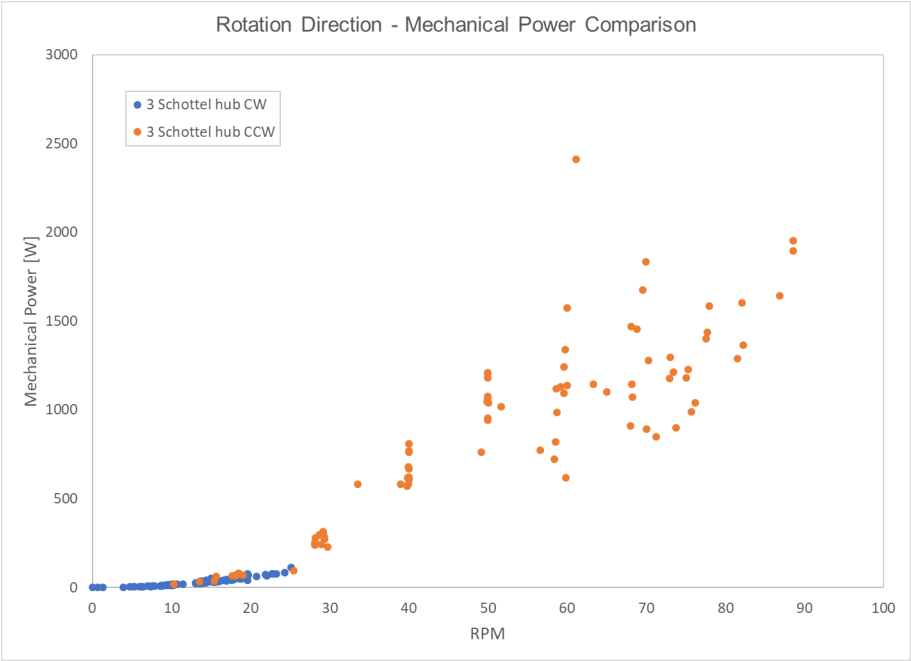

Figure 33 Mechanical power for 3 Schottel hub rotating CCW compared with CW.

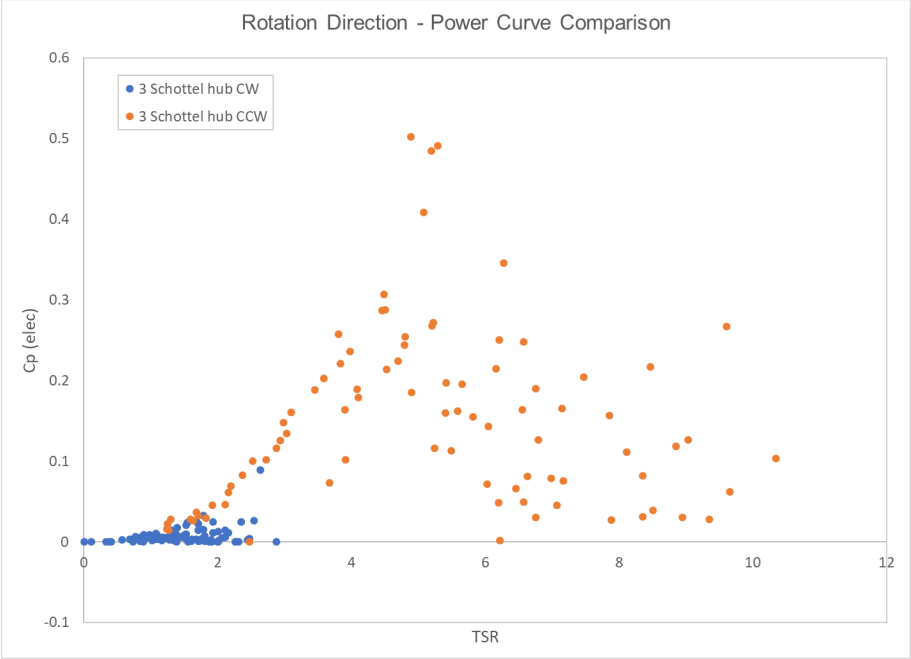

Figure 34 Coefficient of electrical power for 3 Schottel hub rotating CCW compared with CW.

When the Schottel blades were tested in the clockwise (CW) direction, two different pitch angles, 12° and 24°, were tested. The relationship between mechanical power and RPM was determined for both angles (Figure 35 and Figure 36).

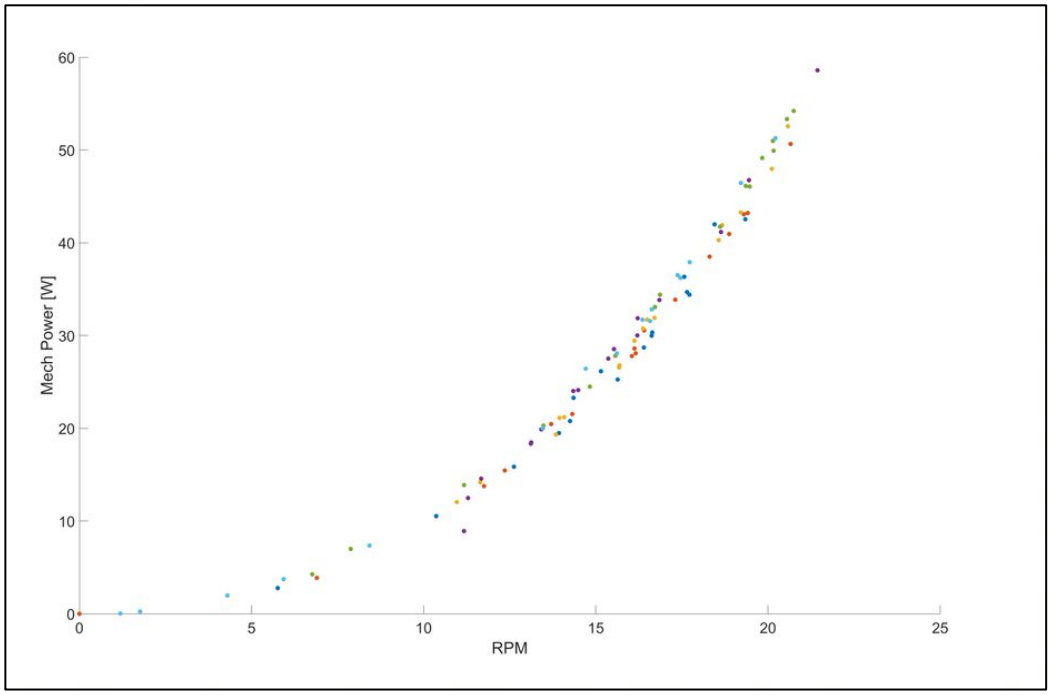

Figure 35 Mechanical Power vs RPM for 3 Schottel hub CW with blade at 12˚

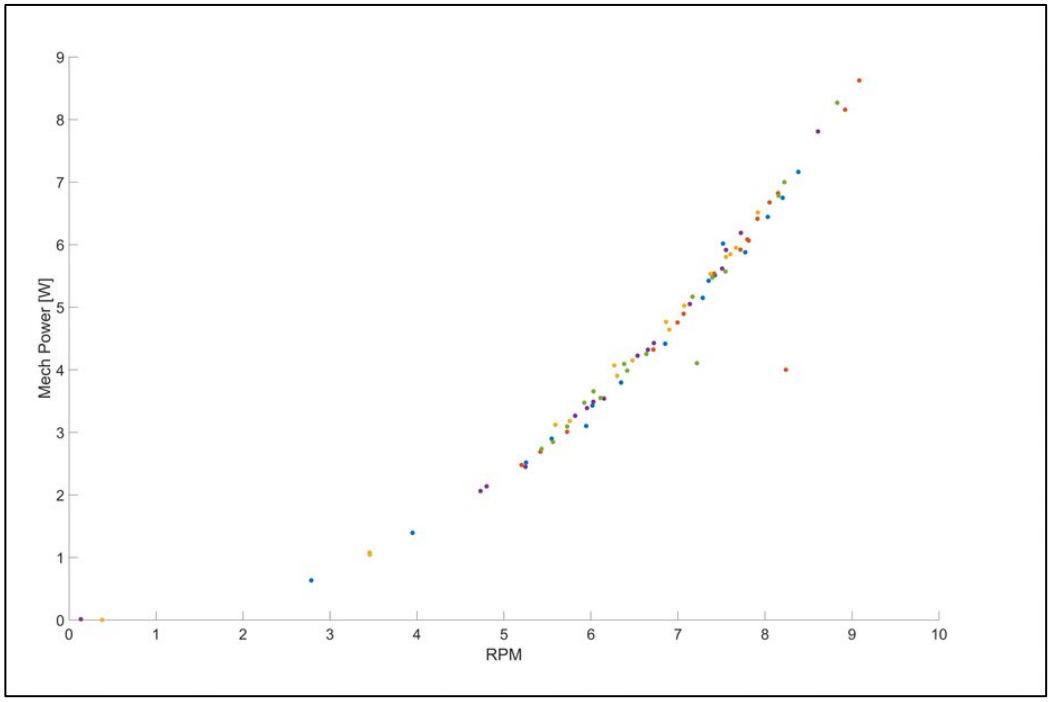

Figure 36 Mechanical Power vs RPM for 3 Schottel hub CW with blade at 24

4 FML hub

Results from testing the 4 FML hub are presented in Figure 37. It is important to note; the traditional nosecone fell off the turbine in the middle of the second test.

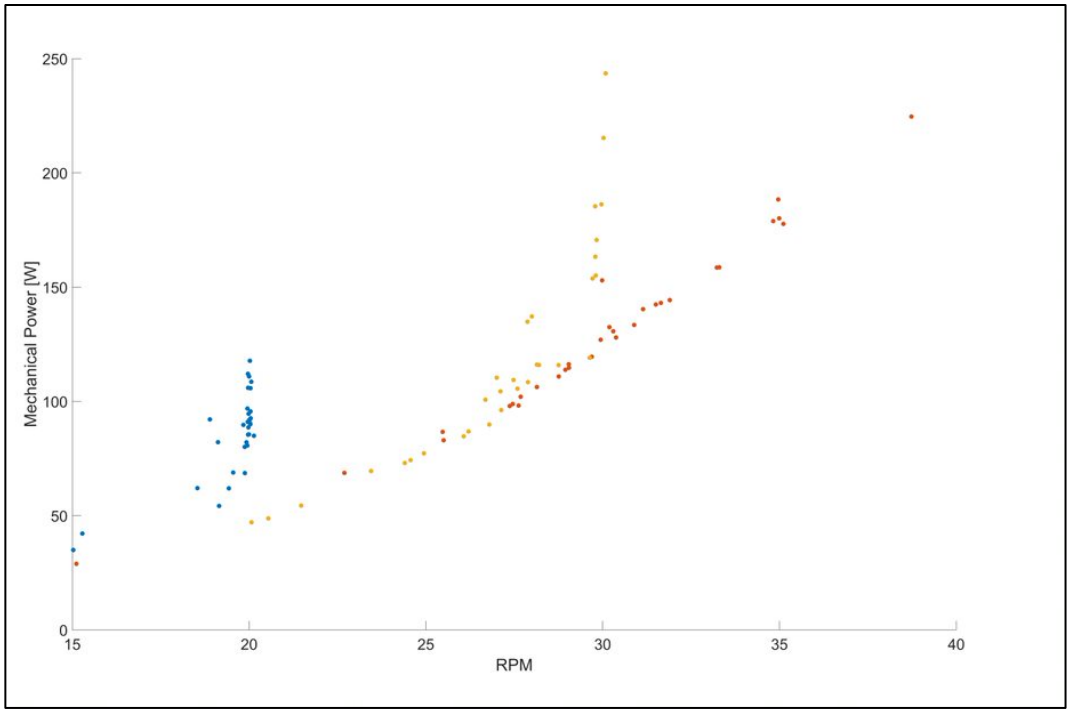

Figure 37 Mechanical power vs RPM for 4 FML hub

3 Schottel hub without and with PowerCone

The PowerCone was attached to the 3 Schottel hub and this configuration was tested in the CW direction. The mechanical power vs RPM trend was calculated (Figure 38), then both 3 Schottel hub configurations were plotted on the same graph (Figure 39) for a direct comparison.

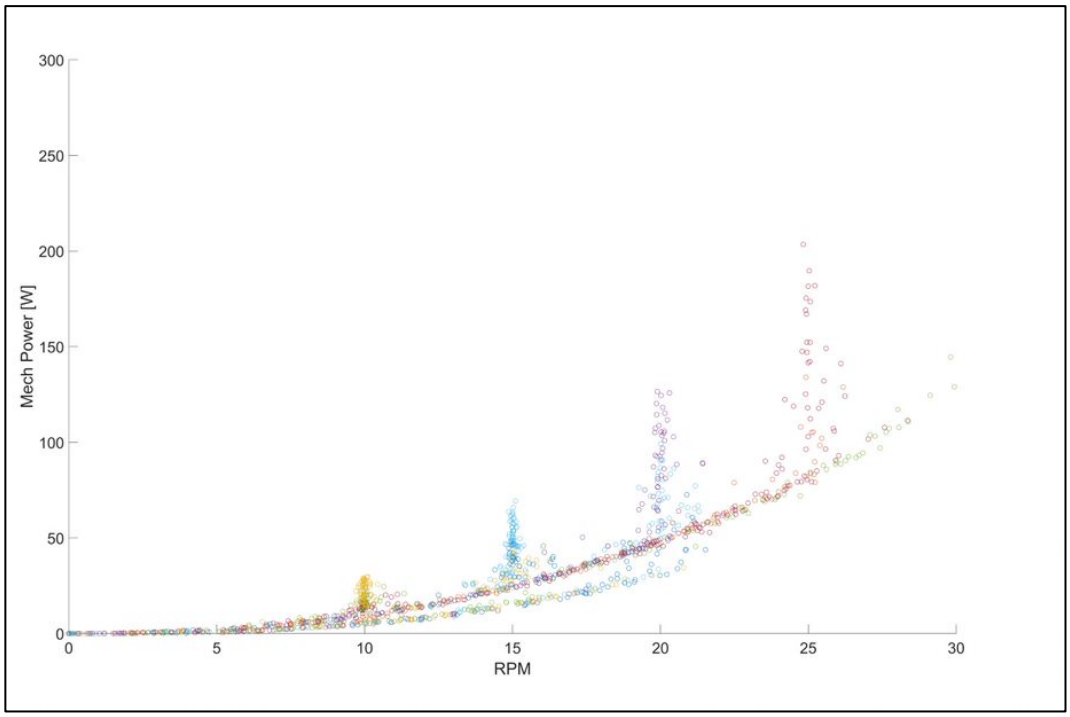

Figure 38 Mechanical Power vs RPM for 3 Schottel hub with PowerCone

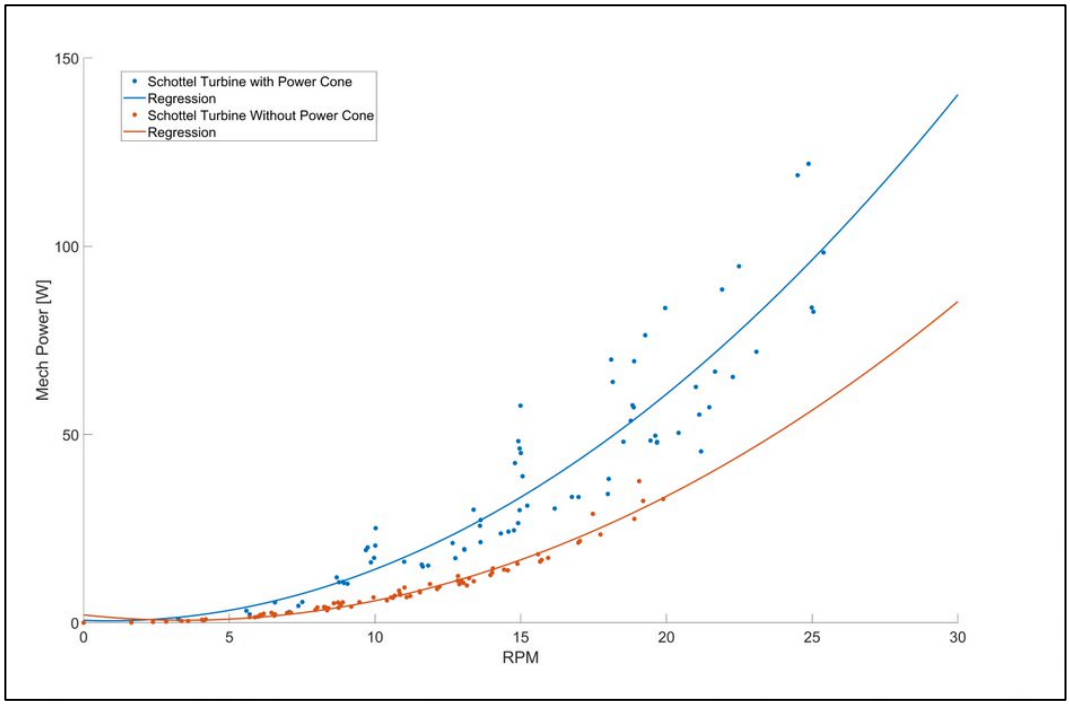

Figure 39 Mechanical power vs RPM for 3 Schottel hub with and without PowerCone

3 Eppler hub or M-hub with and without PowerCone

Three Eppler blades perpendicular to the hub with no PowerCone (3 Eppler hub) were tested. This data will be used as a baseline for comparison with the other configurations. An accelerometer was also attached to the Eppler blades to compare to the accelerometer data from the FML blades. Mechanical power as a function of RPM is shown in Figure 40.

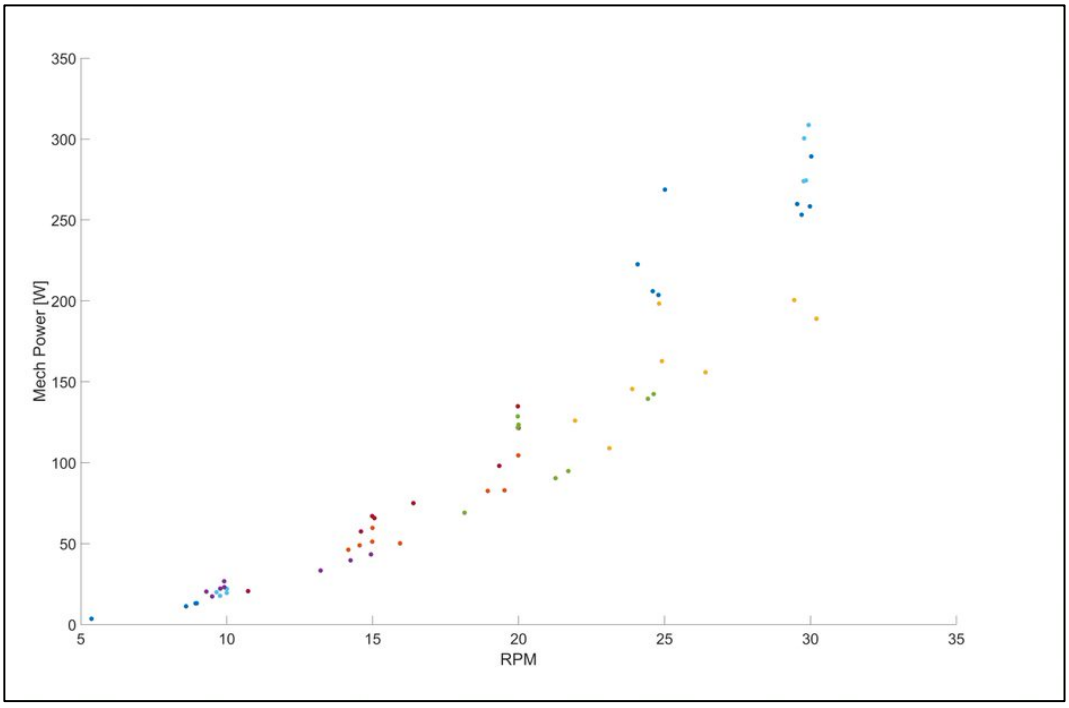

Figure 40 Mechanical power vs RPM for 3 Eppler hub

The M-hub with the three Eppler blades angled back at 60°, and no PowerCone (3 Eppler M-hub) was tested. The mechanical power vs RPM trend was determined (Figure 41).

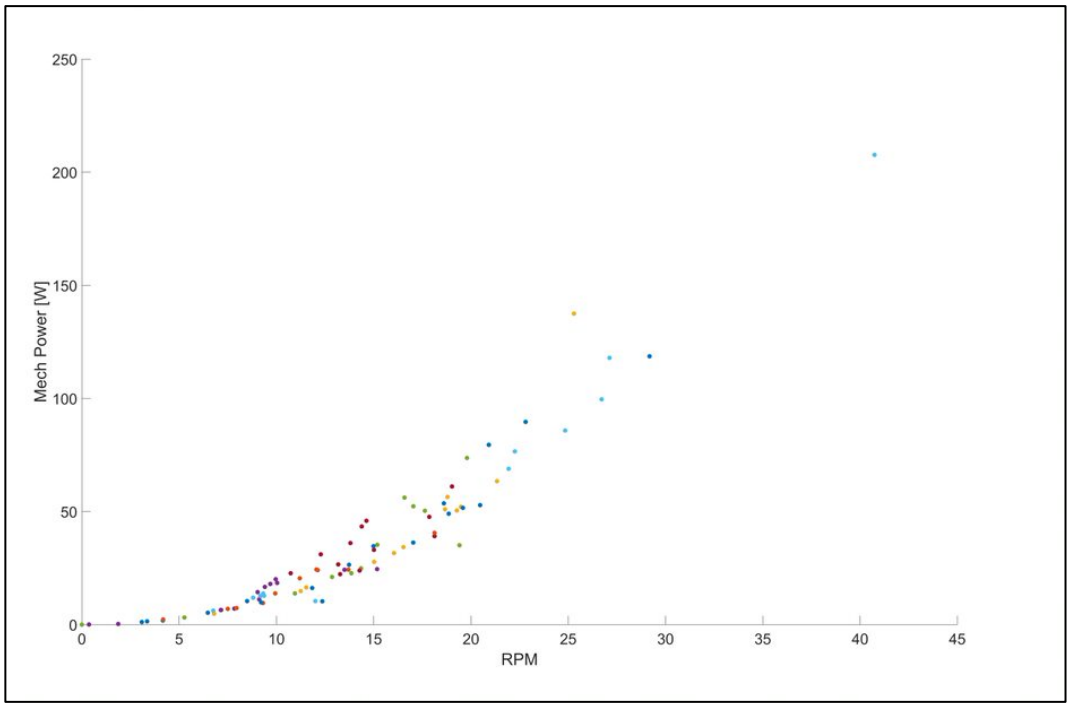

Figure 41 Mechanical power vs RPM for the 3 Eppler M-hub no PowerCone.

The M-hub with the three Eppler blades angled back at 60° with the PowerCone (3 Eppler M-hub PCone) was tested. Mechanical power vs RPM was determined (Figure 42).

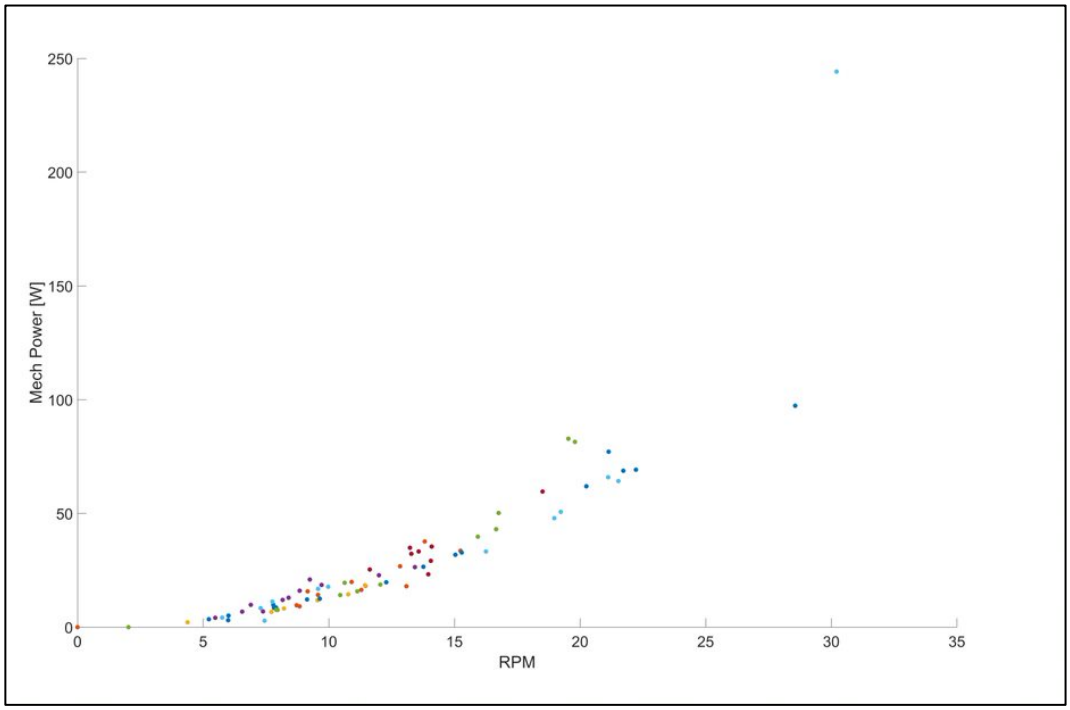

Figure 42 Mechanical power vs RPM for the 3 Eppler M-hub PCone

Data was plotted on the same graph to compare performance between the different blade configurations. The 3 Eppler M-hub with the PowerCone, without the PowerCone and the 3 Eppler hub were compared using power density (Figure 43). Mechanical power per swept area was calculated because the three blade configurations had different swept areas. In addition, the 3 Eppler M-hub with PowerCone was compared to the same hub without PowerCone (Figure 44).

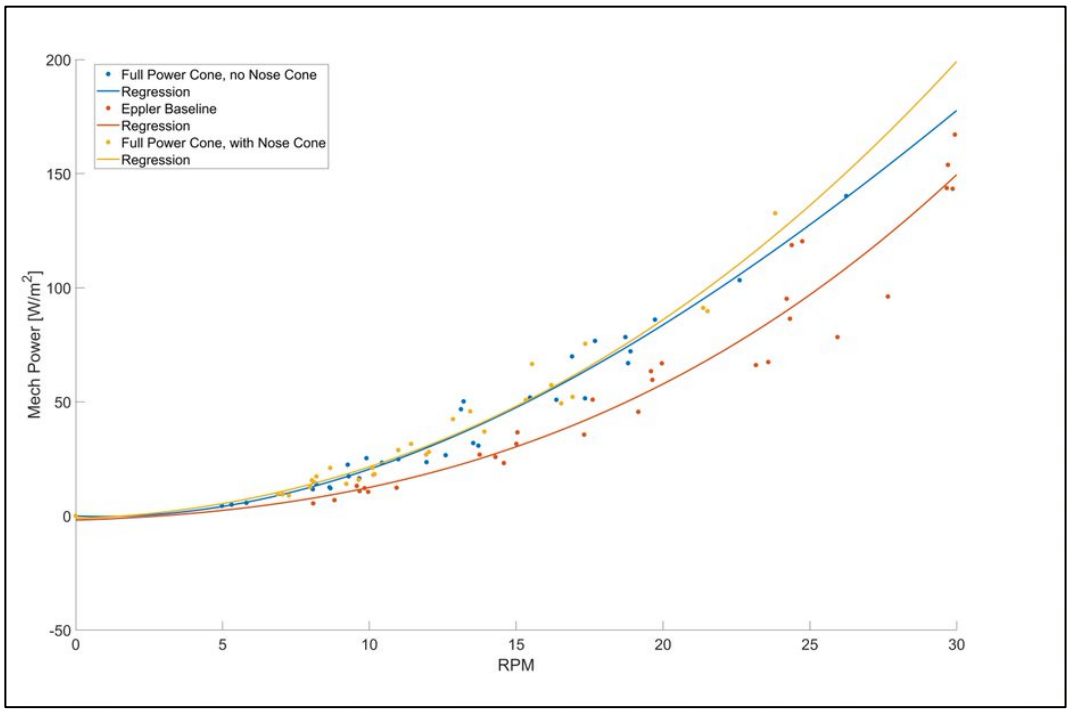

Figure 43 Mechanical power per swept area as a function of RPM for 3 Eppler M-hub with and without PowerCone and 3 Eppler hub

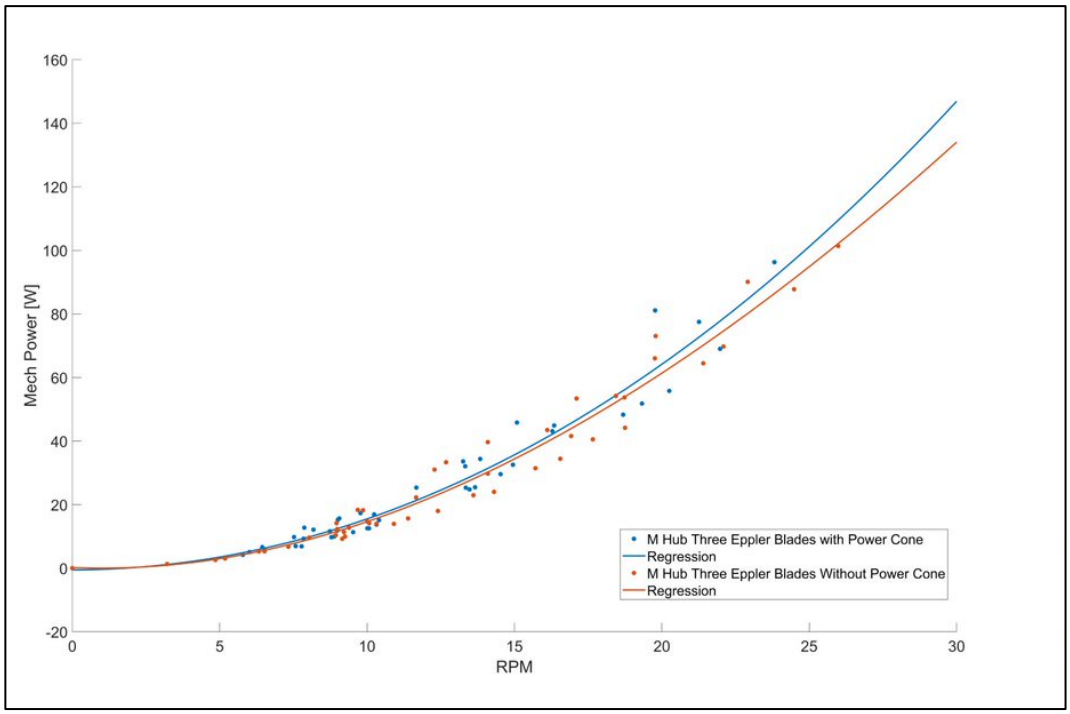

Figure 44 Mechanical power vs RPM for 3 Eppler M-hub with and without the PowerCone

Thrust loads

Thrust loads were calculated from the thrust pin voltage data collected by the DAQ system. The calibration equation is Thrust [N] = (x [V] – b)/m, where b = 1.4781 and m = 0.0144. The linear regression analysis on the calibration had R^2 = 0.9407. Thrust data for the various configurations is presented in Figure 45 through Figure 47.

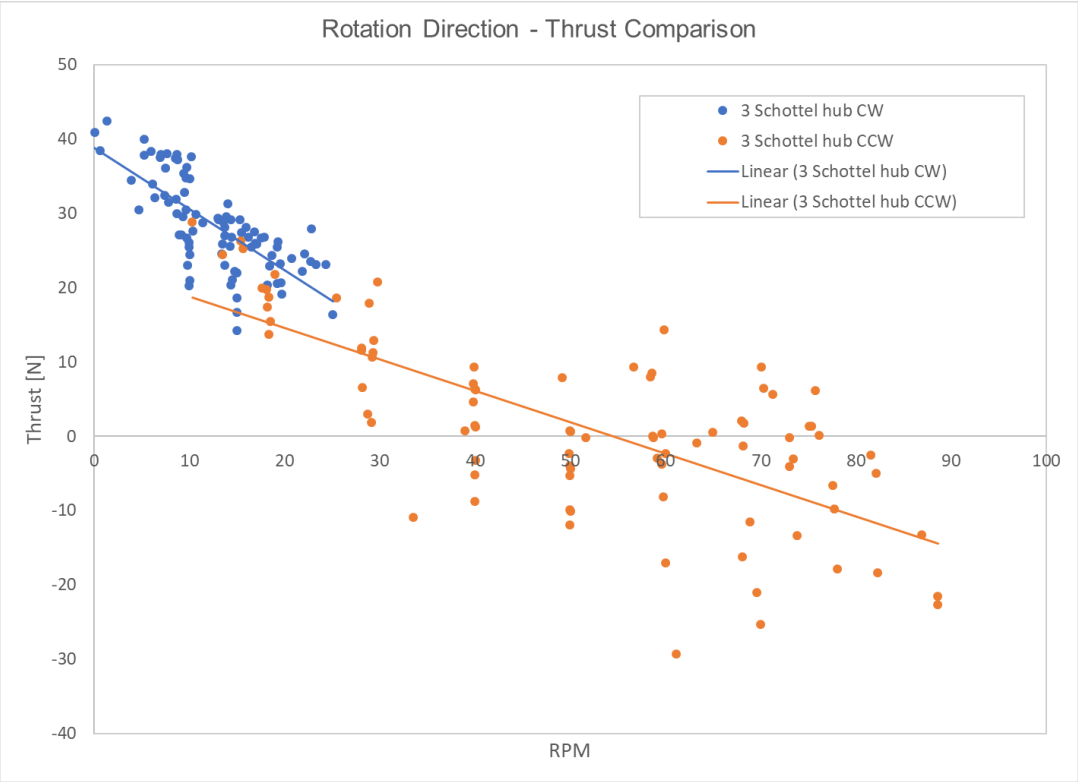

Figure 45 Thrust for 3 Schottel hub rotating CW and CCW

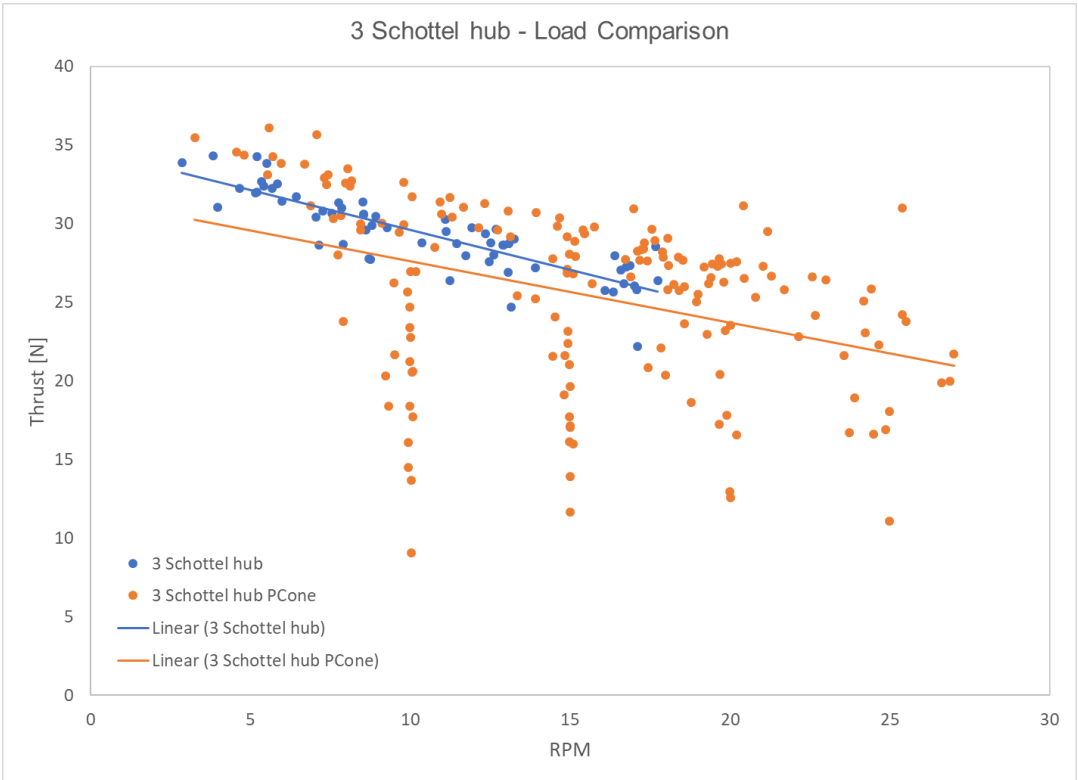

Figure 46 Thrust for 3 Schottel hub with and without PowerCone

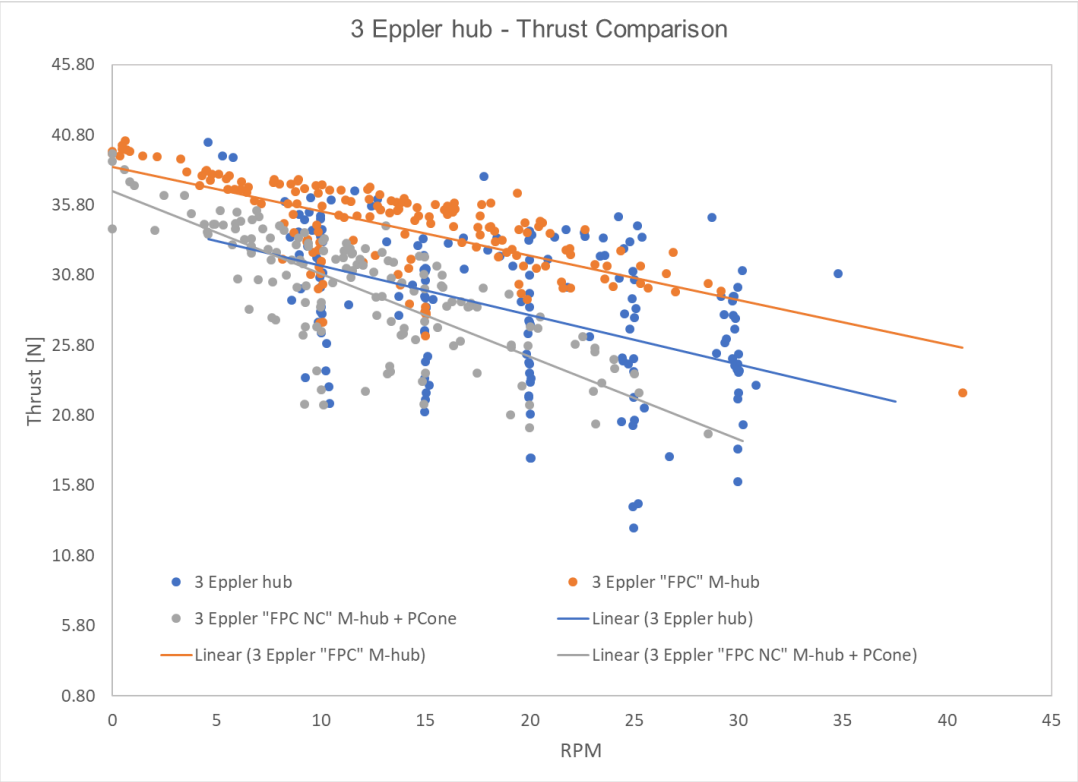

Figure 47 Thrust for 3 Eppler hub and 3 Eppler M-hub with and without PowerCone

Comparison of Configurations – Mechanical Power

Figure 48 Mechanical Power versus Flow velocity for a number of configurations

Figure 48 shows an example of the mechanical power data versus inflow velocity. While the mechanical power was less reliable than the electric power, the data set does show some interesting trends. It appears to show that in turbulent flow the curves for the turbines with the PowerCone are more defined and that data is more coherent.

Discussion

Power curves using $C_{p(mech)} - \lambda$ were calculated for the tests, however, the $C_{p(mech)}$ values were at times greater than one. It is impossible for the turbine to convert all or more of the flow power into mechanical power. This is evidence of systematic error in the measurements where the calculated mechanical power was too large compared to the power available in the flow. The torque meter was calibrated every morning before tests, it is possible that the torque meter became uncalibrated over the course of the day. Therefore, power curves were evaluated using $C_{p(elec)} - \lambda$ and the results were more realistic.

The general bell curve relationship for power curves can be observed in Figure 32 for the 3 blade Schottel CCW hub. The maximum electrical coefficient of power was 0.25 at approximately TSR = 4.5. This is less than the power curve generated in papers from Carwyn Frost which had a maximum of about $C_{p(mech)}$= 0.44 at TSR = 4.5 (Frost et al. 2017). Note that the coefficient of mechanical power was used in Carwyn Frosts papers, not coefficient of electrical power. The efficiency of the generator and the amount of mechanical power converted into electrical power needs to be studied to accurately compare $C_{p(mech)}$ and $C_{p(elec)}$. In addition, there are a considerable number of anomalies in the data points after tip to speed ratio became greater than 4. This is indicative of the turbulent effect of the water flow since the speed of the water in the direction perpendicular to the turbine blades varied greatly. When observing the raw data, the water speed changed from 0.3m/s to 1.2m/s in the span of half of a second. This highly variant flow speed means a larger range of TSR but limited the ability of the turbine to produce meaningful power because there was water flowing at the rotor from many different random directions. Each data point was averaged over 60 seconds, the instrumentation recorded measurements 10x and 15x every second (10Hz and 15Hz) for the turbine and Vector respectively. An average over 60 seconds

for every data point, which is 600 – 900 measurements, is a relatively large data set for just one point. On average, the flow was approximately consistent from 0.6-0.8 m/s, however, there was a large variability and standard deviation. In Figure 32, when the speed of the flow compared to the speed at the tip of the turbine blade was greater or more by a factor of 4 (TSR > 4), the turbine had much more inconsistency in mechanical power produced. This is due to the highly variable flow speed and the lag between the Vector and turbine and the inability of the turbine to maintain set RPM. There were also some data points that had a tip to speed ratio greater than 10. This is because there could have been an instantaneous data point with large flow speed in a span of lower flow speeds and lower rotational blade speed.

The control system removes the electrical load of the generator on the rotor hub to help speed it up and maintain it at the set RPM. From the data, it can be observed that the turbine had trouble maintaining a high RPM and the electrical load of the generator was often removed. The only blade configuration that was capable of operating at high RPM's was the three blade Schottel hub CCW with the flow. This setup was tested on a range of 20-90RPM, whereas all the other configurations were tested on a range of 20-40RPM. No electrical power is produced when the electrical load is removed, therefore, the coefficient of electrical power becomes zero ($C_{p(elec)} = 0$). This is apparent in Figure 39 for the three blade Schottel hub in the CW direction where there's a significant number of data points that show coefficient of electrical power equal to zero. As mentioned before, the three blade Schottel hub was optimised for rotation in the CCW direction with the flow and the results confirm this when comparing Figure 32 and Figure 39. The CW direction had a maximum of about Cp = 0.1 at TSR = 2.75, on the other hand, the CCW direction had a maximum of about Cp = 0.25 at TSR = 4.5. In addition, the data points for the CW direction were much more variable and 'scattered' than in the CCW direction, although the CCW direction still had many anomalies.

The relationship between mechanical power and RPM for the Schottel blades CCW in Figure 31 was linear as expected and generated a maximum of 1750W at 70RPM. However, the data was not very accurate since there is a large variance in the data points at each set RPM. This is possibly

due to the torque meter losing calibration over the day, turbulence affecting the flow, uncertainty in the instrumentation devices and the lag (distance) between the Vector and turbine rotor. Also, the data points are not grouped in the higher (>60) range of RPM because the turbine and its control system had difficulty maintain higher RPM's.

The mechanical power vs RPM trend was calculated for the Schottel blades in the CW with the flow with two different blade pitch angles: 12° and 24° in Figure 35 and Figure 36. The trend was linear as expected and the turbine clearly performed better with the blades pitched at 12° This orientation generated a maximum of 58W of power at 22RPM compared to just 8.8W at 9RPM for the 24° blades.

A power curve was created from one set of Schottel blades in the CCW direction at 50RPM in Figure 32. There is a slight bell curve that can be observed in the 2 – 6 TSR range, however there are also a lot of data points for TSR higher than 6 with coefficient of electrical power up to 0.55, which is unrealistic for a tidal turbine. This is the result of high spatial variance in the flow and measurement uncertainty.

The performance of the fiber metal laminate blades was evaluated in Figure 37. This turbine configuration operated as expected with a linear trend for mechanical power vs RPM in Figure 39 and Figure 40. Nevertheless, there was a lot of variance and uncertainty in addition to different linear slopes for each set RPM. A maximum of 250 W was generated at 34 RPM, yet this data point was an anomaly separated from the general trend. The power curve determined for the FML blades in Figure 38 barely resembled the expected bell curve relationship and performed very poorly with a maximum 0.25 Cp at 3.7 TSR, which again was an anomaly separated from the general trend closer to 0.1 Cp. The fact that the nosecone fell off and was not installed for the remainder of the data collection could have contributed to variance in the plots and the second smaller slope that can be observed at 20 RPM in Figure 39.

The vibrations in the blades was successfully measured with the accelerometer on the FML blades and Eppler blades. The accelerometer also measured the vibrations from the impact testing. The data analysis for this study is ongoing.

The three Schottel blades hub in CW direction was tested with and without the PowerCone. The respective performance for their mechanical power vs RPM trends is presented in Figure 38 and Figure 39. The trend is linear and at first glance, the slope of the trend seems steeper in Figure 38. But the scale on the x axis is different. The configuration without the PowerCone had a larger maximum performance with 250W at 40RPM, compared to 200W at 25RPM. Figure 39 is a direct comparison for mechanical power vs RPM on the same plot after filters were applied to the data. This graph shows that the turbine performed better with the PowerCone.

The last study of this research project was to compare a three Eppler blade configuration with the blades perpendicular to the hub with no nosecone, three Eppler hub with the blades angled back 60° with no nosecone and three Eppler hub with the blades angled back 60° with PowerCone. Figure 40, Figure 41 and Figure 42 show the mechanical power vs RPM trend for these respective configurations. The perpendicular blades had a maximum performance of 300W at 30RPM, the blades angled back with no nosecone had 125W at 30RPM and the blades angled back with the PowerCone had 100W at 30RPM. These hub configurations had different swept areas, therefore a direct comparison with mechanical power per area, after the data was filtered of anomalies, was plotted in Figure 43. According to this graph, the three blade Eppler hub with the blades angled back and the PowerCone performed best. This is confirmed in Figure 44, where the three Eppler hub with the blades angled with and without PowerCone was compared for mechanical power vs RPM. The trend was linear in these graphs as expected with some variation in the data points.

The sources of error in this project with the turbulent nature of the flow created a lot of variance and uncertainty in the plot. The most important improvement for this research project would be to conduct testing in a larger tank or open water site where the flow is more ordered. This would improve the quality and consistency of the data and improve the reliability of the comparisons.

Improving the calibration of the torquemeter, taking into account the distance between the Vector and turbine rotor in the data analysis and reducing oscillations on the Vector would be a few other improvements for this project.

Conclusion

The experimental work presented in this paper successfully compared the performance of the 1/10 scale Schottel turbine with different blade configurations, the performance and resistance to impact of the Fiber Metal Laminate Material blades, and the performance of the turbine with the PowerCone attachment.

At this point it cannot be conclusively determined which one of the blade configurations: the Schottel blades, the Eppler blades, or the FML material blades, had a higher performance.

Regarding the impact of the PowerCone however, the three Schottel blades with the PowerCone attached had a higher mechanical power than the Schottel blades without the PowerCone attached. The Eppler blades when angled back on the M-hub had a higher mechanical power per swept area with the PowerCone attached than the Eppler blades when angled back on the M-hub without the PowerCone, and the Eppler blades perpendicular to the M-hub. Therefore, the PowerCone attachment did improve the performance of the turbine in relation to producing more mechanical power when attached to the turbine. The three Schottel blade hub in the CW direction clearly generated the most power and was capable of operating at much higher RPMs.

The data from the turbines fitted with the PowerCone were more comparable and consistent with expected turbine power curves. There was considerably more scatter in the data points in the turbine configurations tested without the PowerCone. This implies that the PowerCone performed better and produced more reliable power in the turbulent flow than the other turbine configurations.

Further testing of this turbine is needed since the 300 m^3 rectangular ballast tank used for this experiment had high water turbulence, with highly variable flow. While this tank was valuable and useable for comparing the performance of different turbine configurations, it was not a reliable source of absolute performance values.

It is worth investigating if the pool tank at the Aquatron could be used in future experiments and wold have less turbulent flow. This pool tank has been used in the past for tidal turbine-animal interaction work and could be an attractive location for a lab-based animal study that can be paired with a performance test. MacNeill et al. (2017) tested the interaction of a small vertical axis turbine (1m in diameter) with Striped bass (*Morone saxatilis*) within the 15.24m diameter pool tank. Furthermore, the performance of the vertical axis turbine was validated against towing tank experiments done at the National Research Council (NRC), St. John's, and it was determined that the flow in the pool tank was close to the inflow site for the flow speed range tested (MacNeill et al. 2017). Continued development of tidal turbine testing in controlled laboratory environments is still needed and controlling a consistent flow will be critical in future testing.

The opportunity for the PowerCone in the tidal power industry is quite broad. The PowerCone could add considerable value to projects if the results above are validated. Further investigation of the PowerCone would give absolute performance values that are needed for AEP estimations. The increased efficiency, lower cut in speed and consistent power in turbulent flow mean:

Increased AEP

Ability to economically deploy in lower speed sites

Ability to deploy in turbulent sites

Ability to deploy in rivers with shorter 'straight' sections

Ability to deploy in sites with irregular ocean or river floors.

The PowerCone could drive opportunities for developers in the many global sites that have lower current speeds and imperfect site conditions.

References

Asaee, Z., Mohamed, M., De Cicco, D., Taheri, F., (2017). "Low-Velocity Impact Response and Damage Mechanism of 3D Fiber-Metal Laminates Reinforced with Amino-Functionalized Graphene Nanoplatelets," International Journal of Composite Materials 7, 20-36

Asaee, Z., Shadlou, S., Taheri, F., (2015). "Low-velocity impact response of fiberglass/magnesium FMLs with a new 3D fiberglass fabric," Composite Structures 122, 155–165

Asaee, Z., Taheri, F., (2016) "Experimental and numerical investigation into the influence of stacking sequence on the low-velocity impact response of new 3D FMLs," Composite Structures 140, 136–146

Broome JE, Redden AM, Keyser FM, Stokesbury MJW, Bradford RG. (2015). Passive acoustic telemetry detection of striped bass at the FORCE TISEC test site in Minas Passage, Nova Scotia, Canada. Pro- ceedings of the 3rd Marine Energy Technology Symposium, METS2015, April 27–29, 2015, Washing- ton, D.C., USA.

Dalhousie University, Aquatron Laboratory. https://www.dal.ca/dept/aquatron.html.

De Cicco, D., Asaee, Z., Taheri F., (2017). "Low-velocity impact damage response of fiberglass/magnesium fiber-metal laminates under different size and shape impactors, Mechanics of Advanced Materials and Structures, 24, 545-555

Desplanque C, M.ossman DJ. (2001). Bay of Fundy tides. Geoscience Canada. 28:1. 1-11.

DFO (Fisheries and Ocean Canada). (2018). Review of Existing Scientific Literature to Determine the Level of Fish Mortality and Potential Impacts on Fish Populations as a result of the Operation of the Annapolis Tidal Power Facility. Regional Science Response Process-Maritimes Region. http://www.dfo-mpo.gc.ca/csas-sccs/Schedule-Horraire/2019/01_09-10-eng.html.

Frost C, Benson I, ElsäBer B, Starzmann R, Whittaker T. (2017). Mitigating Uncertainty in Tidal Turbine Performance Characteristics from Experimental Testing. Proceedings of the European Wave & Tidal Energy Conference, Cork, Ireland. Vol. 27.

Frost C, Beson I, Jeffcoate P, Elsäßer B, Whittaker T. (2018). The Effect of Control Strategy on Tidal Stream Turbine Performance in Laboratory and Field Experiments. Energies. 11: 1533.

Garrett C. (1972). Tidal Resonance in the Bay of Fundy and Gulf of Maine. Nature. 238. 441–443.

Jeffcoate P, Whittaker T, Boake C, Elsaesser B. (2016). Field tests of multiple 1/10 scale tidal turbines in steady flows. Renewable Energy 87: 240 – 252.

Karunathilake H, Perera P, Ruparathna R, Hewage K, Sadiq R. (2018). Renewable energy integration into community energy systems: A case study of new urban residential development. Journal of Cleaner Production. 173: 292-307.

Lohrman A, Cabrera R, Kraus N. (1994) Acoustic-Doppler Velocimeter for Laboratory Use. https://www.nortekgroup.com/assets/documents/Acoustic-Doppler-Velocimeter-ADV-for-Laboratory-Use.pdf

MacNeill AM, Mahon-Hodgins L, Eddington J, Batt J, Bibeau E, Kregting L, Molloy S. (2017). Tidal Turbine-Fish Interaction Pilot Study in the Aquatron Controlled Lab Space. Proceedings of the European Wave & Tidal Energy Conference, Cork, Ireland. Vol. 27.

Nova Scotia Power. 2018. Renewable energy on the rise; Nova Scotia Power reaches 29% renewables in 2017. https://www.nspower.ca/en/home/newsroom/news-releases/renewable-energy-on-the-rise.aspx.

Maro J, Farret F.A, Cardoso G, Senter D, Lorensetti M.F. (2015). MPPT of Magnus Wind System with DC Servo Drive for the Cylinders and Boost Converter. Journal of Wind Energy. 2015. 1-10. 10.1155/2015/148680.